

Article

Broadband Spectrum Light-Driven PANI/Au/Beta-Cyclodextrin Nanocomposite and Its Light-Triggered Interfacial Carrier Transfer

Xingfa Ma ^{1,*}, Caiwei Li ¹, Xintao Zhang ¹, Mingjun Gao ¹ and Guang Li ²

¹ School of Environmental and Material Engineering, Center of Advanced Functional Materials, Yantai University, Yantai 264005, China

² National Laboratory of Industrial Control Technology, Institute of Cyber-Systems and Control, College of Control Science and Engineering, Zhejiang University, Hangzhou 310027, China

* Correspondence: xingfama@ytu.edu.cn; Tel.: +86-535-6706038; Fax: +86-535-6902264

Abstract: Polyaniline/Au nanocomposites were synthesized by a novel method. Aniline monomers were loaded in the hydrophobic cavities of beta-cyclodextrin, and a polymerization reaction occurred at the interface of the beta-cyclodextrin cavities and the liquid phase of chloroauric acid. UV-vis absorbance indicated that the nanocomposite covered the range of visible light and NIR (near infrared). The photo-excitation experiment was carried out with typical wavelengths in the visible light (405 nm, 532 nm, and 650 nm) and NIR (780 nm, 808 nm, 980 nm, and 1064 nm) regions (10–200 mW) based on Au inter-digital electrodes on flexible polymer substrates casting a thick film. The nanocomposites exhibited photo-current switching behavior in visible light and NIR. The ratio of on/off was enormously dependent on the power and wavelength of incident light. The robust interface coupling between Au and PANi of the nanocomposite promoted the separation and transfer of electron/hole. The mechanism of carrier generation, separation, and transfer at interfaces of Au/conjugated polymer/non-conjugated small organic molecules by light inducement was discussed at the electron level. The results illustrate that the nanocomposites quickly produced free electrons and holes by low-power incident light, could prevent the recombination of electron/hole pairs to a certain extent, and could overcome the interface barriers between metal, conjugated polymer, and small organic molecules for transfer. This provides a simple and practical approach for developing multi-functional nanocomposites that have the potential act as intelligent nano-carriers, photo-current switches, NIR detectors, and for information storage.

Keywords: polyaniline; Au nanoparticles; nanocomposite; interfacial carrier transfer; external stimuli response; photo-current switching



Citation: Ma, X.; Li, C.; Zhang, X.; Gao, M.; Li, G. Broadband Spectrum Light-Driven PANI/Au/Beta-Cyclodextrin Nanocomposite and Its Light-Triggered Interfacial Carrier Transfer. *Coatings* **2022**, *12*, 1401. <https://doi.org/10.3390/coatings12101401>

Academic Editor: You Seung Rim

Received: 19 August 2022

Accepted: 23 September 2022

Published: 26 September 2022

Publisher's Note: MDPI stays neutral with regard to jurisdictional claims in published maps and institutional affiliations.



Copyright: © 2022 by the authors. Licensee MDPI, Basel, Switzerland. This article is an open access article distributed under the terms and conditions of the Creative Commons Attribution (CC BY) license (<https://creativecommons.org/licenses/by/4.0/>).

1. Introduction

Polyaniline-based nanocomposites have been extensively studied and widely applied in various fields due to their outstanding controlled physical properties and simple synthesis. Some important applications include dye-sensitized solar cells [1,2], fuel cells and fuel generation [3–5], energy storage [6–8], lithium-ion batteries [9–11], high-performance super-capacitors [12–22], flexible photo-detectors [23,24], photo-catalytic hydrogen evolution [25,26], actuation and smart devices [27,28], organic devices and microelectronic circuits [29–36], chemical sensors and biosensors [37–43], photo-catalytic degradation of organic pollutants [44,45], antibacterial and antimicrobial applications [46,47], and so on. In recent years, although good progress on the study of polyaniline (PANI) and its nanocomposites has been obtained, there are still a lot of papers published on the synthesis, properties, and applications of PANi and its nanocomposites.

To tailor performance, PANi is often synthesized in nano/micro-structures or composited with other material. Nano/micro-structured PANi can be synthesized through various chemical methods or electrochemical preparations using several soft or hard templates

to control morphology and properties [48–54]. A series of studies of low-dimensional structured PANi and its organic–inorganic nanocomposites have been carried out in our previous reports [55–59]. Among methods to synthesize PANi, dilute aniline aqueous solution polymerization and interface polymerization are simple, low-cost, and effective approaches for obtaining low-dimensional PANi [49–54]. Among PANi-based nanocomposites, noble metal–PANi nanocomposites generally exhibit some enhanced optical and electrical properties due to surface plasmon resonance and the free electrons of metal nanostructures [60–63]. The electronic interaction between metal nanomaterials and PANi can be controlled or enhanced by interface contact and hybridization.

Among noble metals, Au nanoparticles have received considerable attention in chemical sensors, biosensors, and catalysis because the surface plasmon resonance of Au nanoparticles strongly depends on the size and distance [60–67]. Further, Au nanoparticles have excellent bio-compatibility and low toxicity. Enhancing the surface plasmon resonance of Au nanomaterials in NIR generally requires synthesis of low-dimensional Au nanomaterials with a high aspect ratio. The degree of red-shift to NIR of optical absorbance is enormously dependent on the high aspect ratio of Au low-dimensional materials. This requires a large amount of surfactant as a soft template and Ag⁺ as a direction-controlling agent for growth of low-dimensional Au, and the post-treatment process to remove surfactant is very complex and time-consuming [68–70]. Another method is to prepare low-dimensional Au nanomaterials with a hard template, but this process is also time-consuming. Adding a small amount of Au components in PANi would integrate the multi-functionality of materials and widen applicability in interdisciplinary fields. The synthesis of Au nanoparticles is much more straightforward and low-cost than that of low-dimensional Au nanomaterials. The critical issue is how to widen optical response with a straightforward approach. Generally, a Au precursor (such as chloroauric acid) is reduced with appropriate reducing agents, and then synthesis of the conductive polymer is carried out using various oxidizing agents or different metal precursors. Therefore, a mixture of chloroauric acid and aniline can automatically form Au/PANi nano-composite since chloroauric acid acts as the oxidizing agent and aniline as the reducing agent. Sajid Fazal and coworkers [71] reported gold nanoparticle synthesis aqueously with a cocoa extract that served both as a reducing and stabilizing agent. The resulting product exhibited good absorbance in NIR for photo-thermal treatment and bio-imaging in biomedical fields. It provides a green and simple way to synthesize metal nanomaterials.

Cyclodextrins are typical macro-cycles with unique structure, good bio-compatibility, and recognition and self-assembly ability, and are endowed with fascinating hydrophobic cavities and a hydrophilic surface, which enable the encapsulation of diverse small organic molecules by forming inclusion complexes. The hydrophobic cavities of cyclodextrins can be used as reactive raw material containers for the synthesis of nanomaterials. Cyclodextrins and their derivatives have successfully been applied in recognition [72,73], intelligent sensing [74–80], solid-phase extraction [81–83], construction of intelligent surfaces, sustained drug and gene release [84–104], removal of organic pollutants [105–110], supra-molecular assemblies, and smart devices. To obtain PANi functionalized with cyclodextrins, aniline was loaded in the hydrophobic cavities of beta-cyclodextrin as a reservoir of polymer monomer so that the polymerization occurred at the interface of cavities of beta-cyclodextrin and the liquid phase of oxide agents to avoid exothermic effects. This study focused on measuring the physical response of the nanocomposites to external stimuli, especially photo-current generation in response to weak and different wavelengths of visible light and NIR. In one experiment, cyclodextrins were functionalized with a nanocomposite to enhance their physical properties; in another case, interface optimization between metal nanostructure and organic layers, including conjugated polymers and non-conjugated small organic molecules, was performed to explore the mechanism of the contribution of micro-structure on physical properties. From a material physics point of view, we focused on carrier generation and transfer by light excitation, avoiding the recombination of electron/hole and energy dissipation by scattering effects of elec-

tron/electron (or phonon) based on the state of aggregation, chemical state, and interface of nanocomposites at the electronic level. The relationship between microstructure and properties of nanocomposites was discussed. Photo-thermal effects of nanomaterials contribute to locative heat production by scattering effects. In the fields of devices controlled by light, some references report [111–122] conductance switching, light-induced switching of single-molecule junctions, and charge transport mechanisms. Some molecules, such as azobenzenes, diarylethenes, and spiropyranes, overcrowded alkenes, and so were widely used in light-induced switching of single-molecule devices. This work is especially interesting for designing molecule switching at the atomic or molecular level. However, most materials are composite, containing multiple components and multiple phases. The contributions of component, phase, interface, surface, grain boundary, defects, chemical state, doping, and impurity energy level on the properties are excellent. This study aimed to develop light-controlled nanocomposites, tailoring their behaviors and widening their multi-functional or intelligent properties based on the state of aggregation and interface of nanocomposites at the electronic level. The mechanism of carrier transfer across different interfaces of organic/inorganic hybrid was discussed.

Although the study of polyaniline and its nanocomposite has continued for many years, over the last several years, a large amount of research has continued to emerge, along with new energy and energy storage devices [123–131]. For the construction of chemical sensors and biosensors [132–137] and the development of multi-functional nanocomposites, conjugated conductive polymers are still the crucial material system. For example, Arpit Verma and coworkers [138] studied ZnS nanosheets in a polyaniline matrix as metallopolymer nanohybrids for flexible and bio-friendly photodetectors. Mu-Yi Hua and coworkers [139] focused on the synthesis and characterization of soluble n-doped polyaniline. Han and coworkers [140] prepared polyaniline–silver composite by glucose reduction and examined its properties. Ryo Miyashita and coworkers [141] developed an electro–magneto–optically active polyaniline/hydroxypropyl cellulose composite. Additionally, ultrafiltration membranes, membranes for CO₂ separation, wastewater treatment, and oil/water separation, etc., are also applications for polyaniline-based nanocomposites [142–144]. We focused on separating photo-generated carriers by using the interface interaction between Au nanoparticles and an organic layer in this paper.

2. Materials and Methods

2.1. Materials

Aniline (analytical reagent (AR)), HAuCl₄ (AR), ammonium persulfate (AR), ammonia (CP) (25% purity), hydrochloric acid (AR), and hydroxypropyl-β-cyclodextrin were purchased from Sinopharm Chemical Reagent Co., Ltd (Shanghai, China). Deionized filtered water was used in all studies.

2.2. Loading of Aniline in The Hydrophobic Cavities of Beta-Cyclodextrin

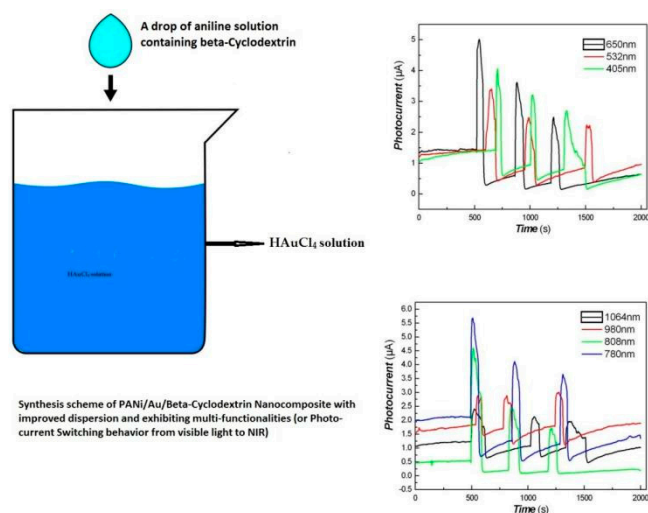
A total of 1 mL aniline was added to 3 g hydroxypropyl-β-cyclodextrin, and the mixture was left standing for 24–72 h at room temperature. Then, 300 mL deionized filtered water was added, and the mixture was left standing for 24–72 h at room temperature. During these periods, hydroxypropyl-β-cyclodextrin dissolved in the water, and the oil droplet of aniline disappeared very slowly. The concentration of hydroxypropyl-β-cyclodextrin was about 10mg/mL.

2.3. Synthesis of Au/Polyaniline Nanocomposite Functionalized with Beta-Cyclodextrin

In the experiment, appropriate chloroauric acid (0.02 M) was added to a 300 or 500 mL glass vessel, and the proper aniline solution containing hydroxypropyl-β-cyclodextrin (about 10mg/mL) was added dropwise; the mixture was left standing for 24 h at room temperature. After the products were washed with deionized water 5–6 times, the nanocomposites were obtained. The changes in the contents of chloroauric acid and hydroxypropyl-β-cyclodextrin are shown in Table 1. The synthesis scheme is shown in Figure 1.

Table 1. Composition of experimental PANi/Au nanocomposite containing beta-cyclodextrin.

Sample No.	Loading Aniline Solution	Loading Chloroauric Acid (0.02 M)	Hydroxypropyl- β -cyclodextrin (about 10mg/mL)	Loading Persulfate Solution (0.02 M)
1	50 mL(0.036 M)	-	0.5 g	50 mL
2	50 mL(0.036 M)	50 mL	0.5 g	-
3	100 mL(0.036 M)	100 mL	1.0 g	-
4 (for comparison)	50 mL(0.02 M)	-	-	50 mL

**Figure 1.** Synthesis scheme of PANi/Au/Beta-cyclodextrin nanocomposite with improved dispersion stability and multi-functionality.

For experiment comparison, 50 mL aniline solution (0.02 M) was added dropwise to 50 mL ammonium persulfate solution (0.02 M) to obtain a sample without hydroxypropyl- β -cyclodextrin, which was left standing for 24 h at room temperature. The products were washed with deionized water 5–6 times, and polyaniline without beta-cyclodextrin was obtained. This is also shown in Table 1.

2.4. Morphology Observations with SEM

Scanning electron microscopy (SEM) observation and energy dispersive spectroscopy (EDS) measurements were performed using a Hitachi S-4800 (HITACHI, Tokyo, Japan). The obtained sample was washed with deionized water, deposited on Al foils, dried at room temperature, and then sputtered with a thin layer of Pt on the surface for SEM observation. The sample for EDS measurements did not need to have a layer of Pt deposited on its surface.

2.5. Morphology Observation with TEM

Transmission electron microscopy (TEM) observation was carried out using a JEM-1011 (JEOL, Tokyo, Japan). The sample solutions were deposited on copper mesh coated with carbon film and dried at room temperature.

2.6. Measurement of UV–Vis Spectrum

Ultraviolet–visible spectroscopy (UV–vis) was performed by a TU-1810 spectrophotometer (Beijing, China) with the samples suspended in water.

2.7. Measurement of FTIR Spectra

Fourier transform infrared spectroscopy (FTIR) was taken with KBr and recorded on an IR Prestige-21 FTIR spectrometer (Beijing, China). The sample and KBr powders were mixed and pressed into a small slice and then dried at room temperature.

2.8. Photo-Responses of Nanocomposite to Visible Light and NIR

The nanocomposite suspension in water was cast on Au inter-digital electrodes on a flexible PET (polyethylene terephthalate) substrate and dried at room temperature. The photo-conductive responses to visible light (white light) (20–25 W; 405 nm, 532 nm, and 650 nm) and low-power NIR (10–200 mW; 780 nm, 808 nm, 980 nm, and 1064 nm) were determined with an LK2000A Electrochemical Work Station (LANLIKE Chemistry and Electron High Technology Co., Ltd., Tianjin, China) applied with 1 V DC bias. The schematic diagram is as follows in Figure 2.

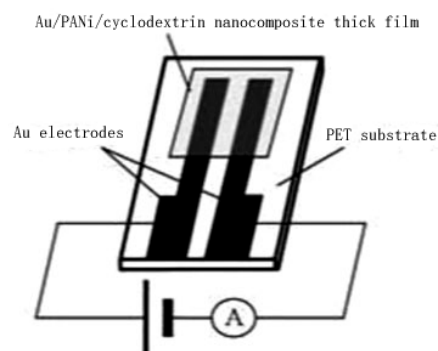


Figure 2. The schematic diagram of the structure of Au electrodes on a flexible polymer substrate.

In this study, the structural schematic diagram of a photo-detector prototype device consisting of organic/inorganic nanocomposite thick film on PET substrate and Au as electrodes was based on [145], who reported that quartz acts as the substrate and the Au gap as electrodes.

3. Results and Discussion

It is well known that cyclodextrins have an interesting structure of hydrophobic cavities and hydrophilic surfaces, which enables the encapsulation of diverse small organic molecules by forming inclusion complexes. Therefore, cyclodextrin cavities can be used as reactive containers. In the experiments, it was found that aniline monomers can be loaded into the hydrophobic cavities of beta-cyclodextrin. Still, the rate of loading was very slow (about 1–3 days) due to the small cavity of beta-cyclodextrin. To examine the morphological evolution of PANI nanocomposite, a series of PANI nanocomposites were synthesized under similar conditions for comparison. The representative SEM images of PANi prepared with dilute aniline aqueous solution polymerization are shown in Figure 3A. Representative SEM images of PANi functionalized with beta-cyclodextrin with novel interface polymerization are shown in Figure 3B,C (different magnification). Representative SEM images of Au/PANi nanocomposite functionalized with beta-cyclodextrin with novel interface polymerization are shown in Figure 4.

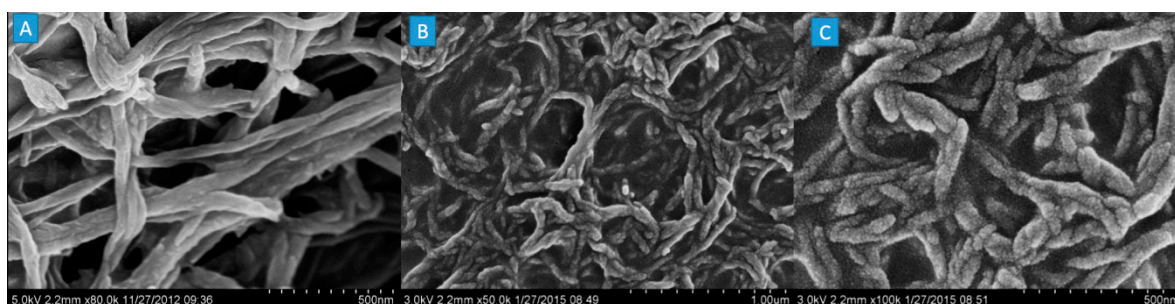


Figure 3. Representative SEM images of series of PANI nanocomposites ((A) Sample 4; (B,C) Sample 1).

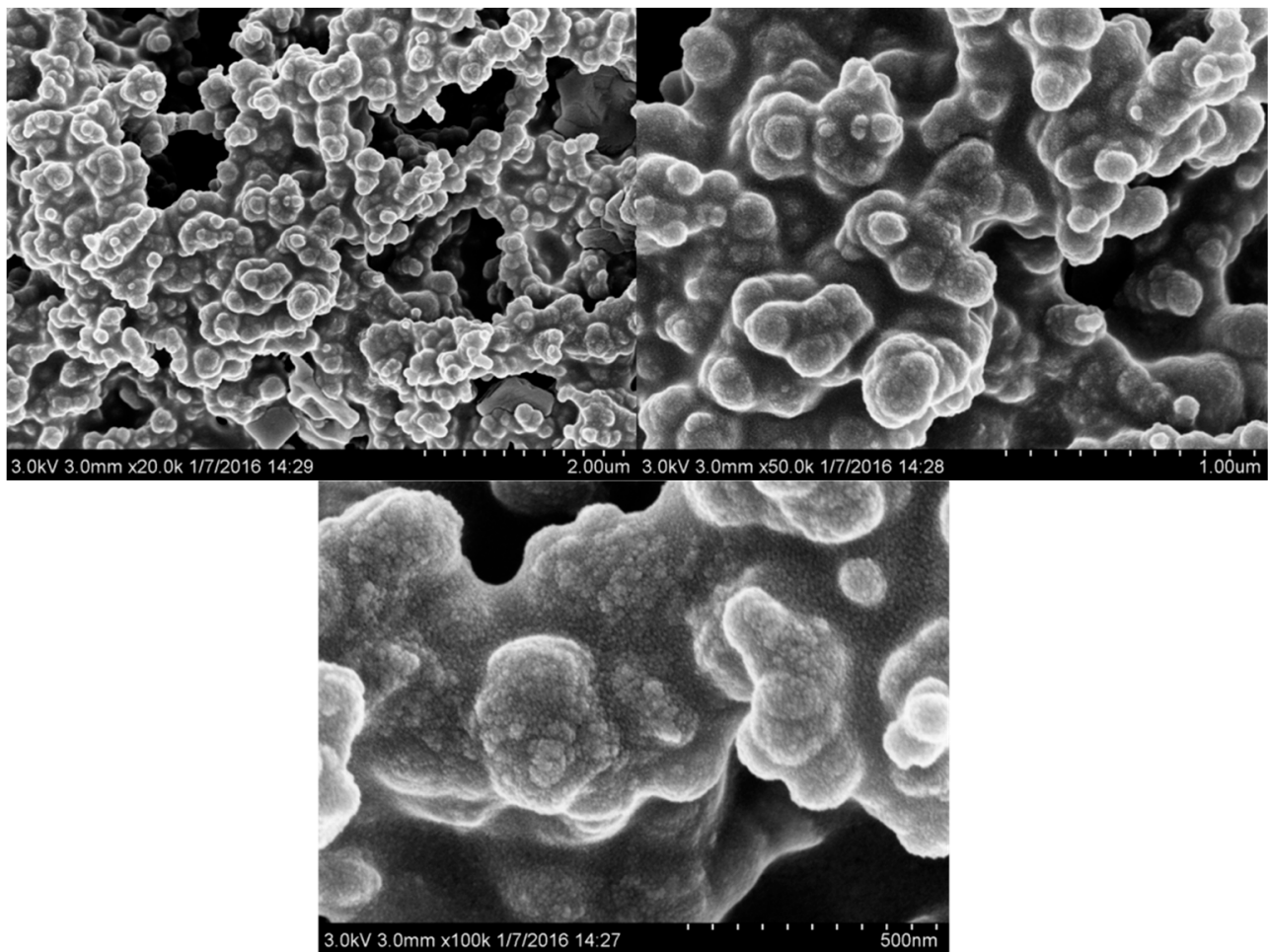


Figure 4. Representative SEM images of Au/PANi nanocomposite functionalized with beta-cyclodextrin with novel interface polymerization (Sample 2) (different magnification).

In comparison with Figure 3, it is found that the PANi morphology is different. Figure 3A shows that the morphology of PANi prepared by dilute aniline aqueous solution polymerization has a nanowire structure, which is consistent with a previous report [51]. Figure 3B,C show that PANi functionalized with beta-cyclodextrin is embedded in the polymer-like film, and the surfaces of PANi nanowires are not smooth but contain many porous structure and small particles. However, they still exhibit nanowire morphology. This illustrates that the formation of PANi nanowire is the result of aggregation of PANi particles due to slow release of aniline from cavities of beta-cyclodextrin compared with dilute aniline aqueous solution polymerization. It is favorable to remove the reactive heat in aniline polymerization. Figure 3A shows the relatively smooth surface of PANi prepared with dilute aniline aqueous solution polymerization. Regarding Au/PANi nanocomposite functionalized with beta-cyclodextrin with novel interface polymerization, Figure 4 shows that the morphology with different magnifications was a nanoparticle structure, and nanoparticles were interconnected with polymer because of Au's specific gravity. This morphology was also supported by TEM examination. Representative TEM images with different magnifications of Au/PANi nanocomposite functionalized with beta-cyclodextrin by novel interface polymerization are shown in Figure 5.

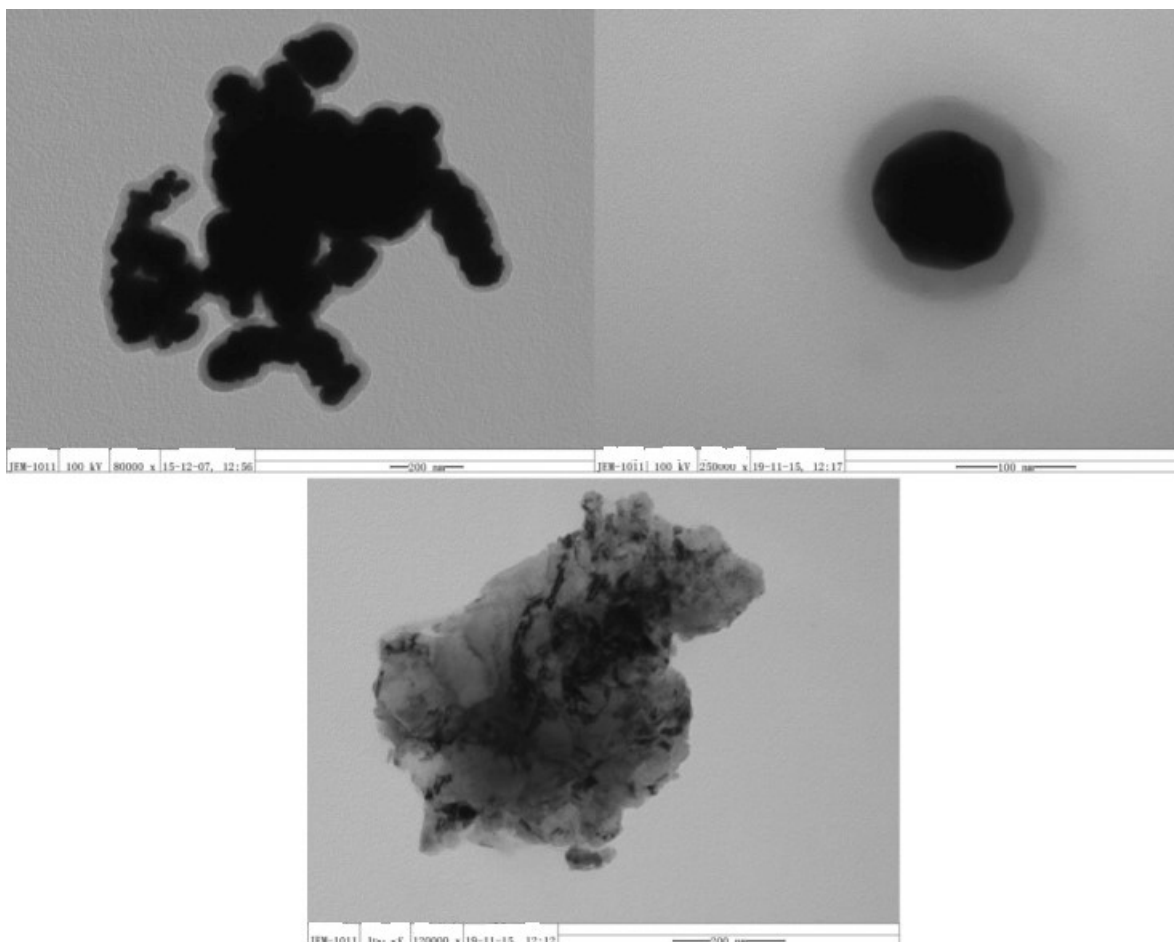


Figure 5. Representative TEM images of Au/PANi nanocomposite functionalized with beta-cyclodextrin with novel interface polymerization (Sample 2).

The border of aggregated particles contained a transparent shell of polymer, which could be the core structure; isolated particles are also clear in this core/shell structure, and the Au nanoparticles are coated with a layer of the organic shell interconnecting with polymer. The thickness of the polymer shell is about 10–20 nm. The organic shell layer contains polyaniline and beta-cyclodextrin. Other morphology could be affirmed as nanomaterials dispersed in the polymer. Due to the formation of Au/PANi appearing at the interface of cavities of beta-cyclodextrin, the cavities of beta-cyclodextrin can be considered small reactors, similar to those of micro-emulsion polymerization in polymer fields. The presence of beta-cyclodextrin also acts to stabilize Au/PANi nanocomposite due to the hydroxy group of cyclodextrin. The dispersion solution of Au/PANi nanoparticles containing hydroxypropyl- β -cyclodextrin has excellent stability in water, and precipitation is challenging and takes a long time. The dispersion effects are very similar to that of our previous report adding a small amount of poly(sodium-p-styrene sulfonate) (PSS) [58]. PSS is a polymer surfactant and is extensively used in self-assembly nano/micro-structures or films, while hydroxypropyl- β -cyclodextrin is a small organic molecular, and its role is similar to that of surfactant with the loading and releasing hydrophobic drugs in biomedical fields. The hydroxy group of cyclodextrin and the H₂O molecule have strong interaction because of the presence of hydrogen bonding, and the cyclodextrin unit also has good compatibility with Au/PANi nanoparticles. Hence, the Au/PANi nanocomposite has good dispersion stability in the water phase due to the presence of hydroxypropyl- β -cyclodextrin.

The FTIR of a series of PANi nanocomposites functionalized with beta-cyclodextrin is shown in Figure 6.

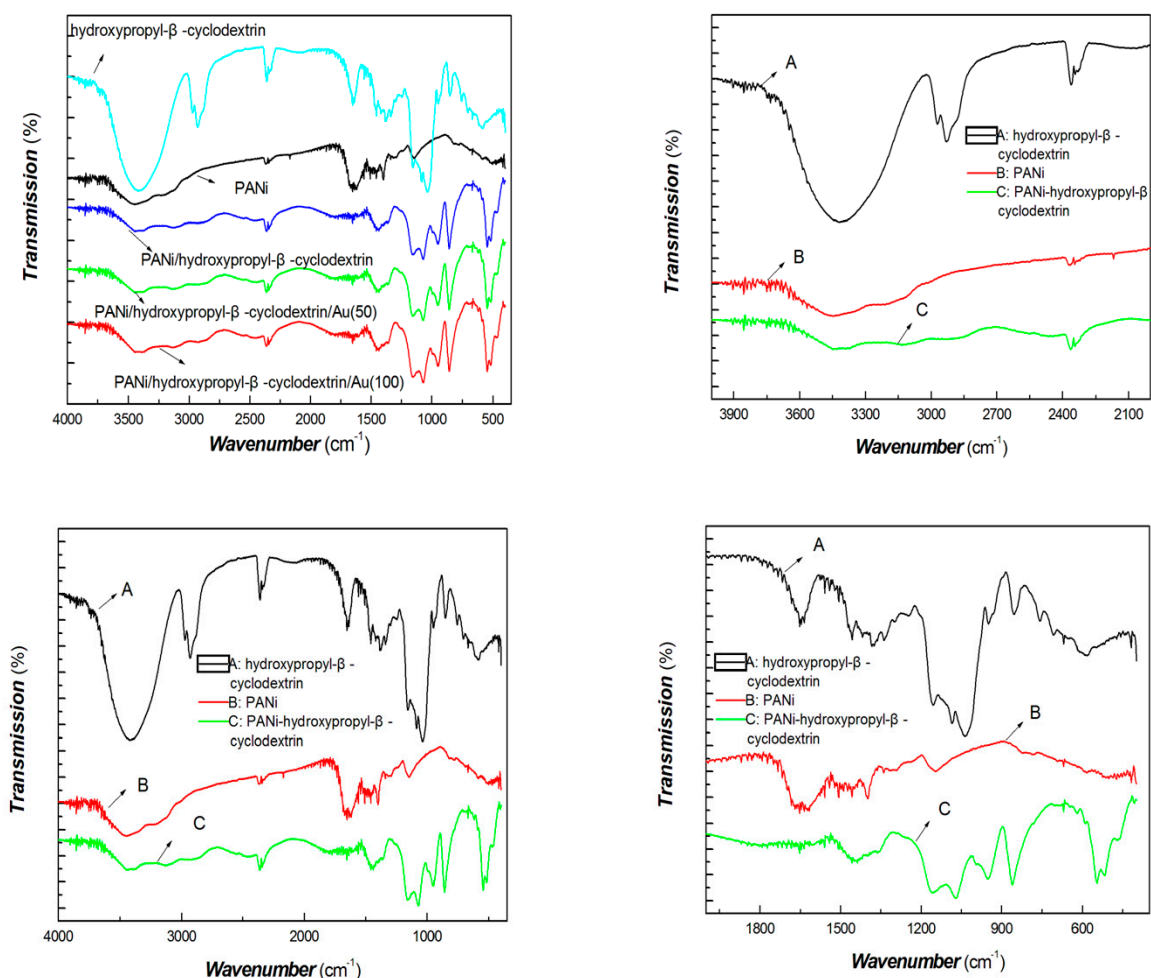


Figure 6. FTIR of a series of Au/PANi nanocomposites functionalized with beta-cyclodextrin, and a local enlargement.

Figure 6 shows that there is no clear difference between the FTIR spectra of PANi/cyclodextrin and PANi/cyclodextrin/Au(50). Likewise, there is little difference between the FTIR spectra of PANi/cyclodextrin/Au(50) and PANi/cyclodextrin/Au(100). A clear difference is present in the samples with and without cyclodextrin. Most absorption bands of FTIR of Au/PANi nanocomposites functionalized with beta-cyclodextrin were located between beta-cyclodextrin and polyaniline. Some bands overlapped with those of beta-cyclodextrin, and others overlapped with those of polyaniline. As shown in Figure 6 of PANi/cyclodextrin/Au(50, 100), the bands at 3415.5 cm^{-1} , 1646.24 cm^{-1} , and 1252.7 cm^{-1} are attributed to the stretching vibration of the $-\text{OH}$ group of cyclodextrin. The wavenumber of 1671.7 cm^{-1} is the stretching vibration of $\text{C}-\text{C}$, and 2924 cm^{-1} belongs to the stretching vibration of CH_2 . The 3436.4 cm^{-1} wavenumber is the stretching vibration of $\text{N}-\text{H}$; 1561.5 cm^{-1} and 1292.3 cm^{-1} are attributed to the stretching vibration of $\text{C}-\text{N}$ of quinonoid and benzenoid rings; 1496.5 cm^{-1} and 1577.6 cm^{-1} belong to the stretching vibration of $\text{C}=\text{C}$ of quinonoid and benzenoid rings. These characteristic bands preliminary illustrate that the nanocomposites contained polyaniline and beta-cyclodextrin components.

As shown in Figure 7, the firm absorbance peaks of PANi functionalized with beta-cyclodextrin at 345 nm or so, 431 nm, and 792 nm are very clear. These absorbance peaks are similar to those previously reported for PANi. The characteristic peaks at 345 nm or so are due to polyaniline benzene ring $\pi-\pi^*$ electronic transition, and the absorbance peaks at 431 nm and 792 nm result from polaron (polaron)- π^* and polaron- π electron transition generation, respectively. The UV-vis curve of Au/PANi nanocomposite functionalized with beta-cyclodextrin is different from that of PANi functionalized with beta-cyclodextrin.

Great blue-shift of the band edge of Au/PANi nanocomposite functionalized with beta-cyclodextrin was observed with increased content of Au (from 792 nm shifted to 556.2 nm and 664.7 nm, respectively) due to quantum confinement of Au nanoparticle depending on the added contents. These are mainly the results of strong plasma resonance properties and quantum confinement effects of Au nanoparticles. It is well-known that Au nanoparticles have a strong plasma resonance peak of about 523 nm in the visible region. Therefore, a great blue-shift of the band edge of Au/PANi nanocomposite functionalized with beta-cyclodextrin was observed because of quantum confinement of Au nanoparticles.

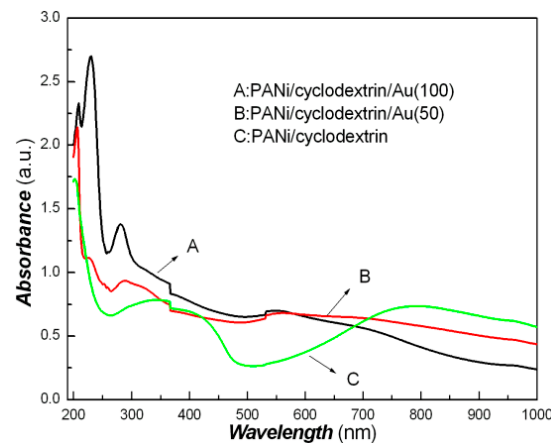


Figure 7. Representative UV-vis spectroscopy of a series of Au/PANi nanocomposites functionalized with beta-cyclodextrin.

XRD of Au/PANi nanocomposites functionalized with beta-cyclodextrin was examined. The results are shown in Figure 8.

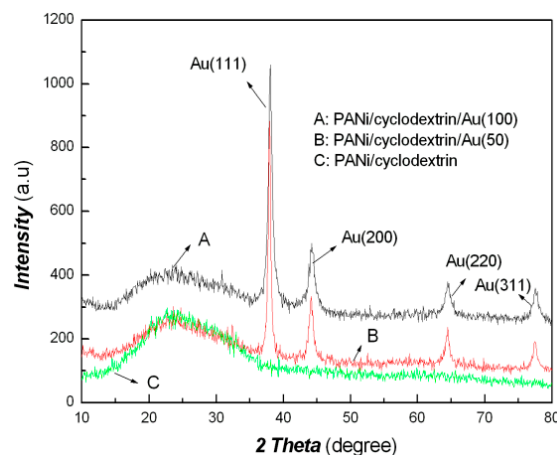


Figure 8. Representative XRD of a series of Au/PANi nanocomposites functionalized with beta-cyclodextrin (A: PANi/cyclodextrin/Au (100); B: PANi/cyclodextrin/Au (50); C: PANi/cyclodextrin).

As shown in Figure 8, spectrum C shows that PANi functionalized with beta-cyclodextrin was an amorphous structure due to no pronounced diffraction peaks. Figure 8 spectrum A and B show that Au/PANi nanocomposite functionalized with beta-cyclodextrin containing different contents of Au nanoparticles had some firm peaks of 2θ in 38.04 (111), 44.22 (200), 64.69 (220), and 77.50 (311). These peaks are the face-centered cubic of Au (PDF#04-0784).

To further confirm the presence of Au in the Au/PANi nanocomposites functionalized with beta-cyclodextrin, EDS of one microdomain containing Au nanoparticles of PANi/Au (100) nanocomposites functionalized with beta-cyclodextrin was determined. The results are shown in Figure 9.

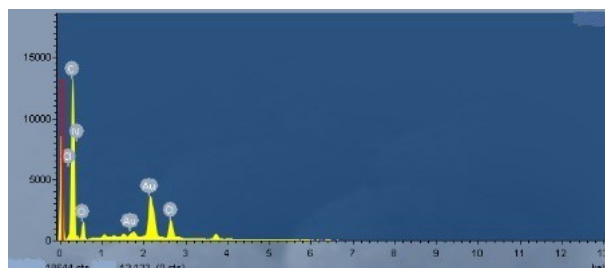


Figure 9. EDS results of one microdomain containing Au nanoparticles of Au/PANi nanocomposites functionalized with beta-cyclodextrin.

Figure 9 shows that the Au/PANi nanocomposites functionalized with beta-cyclodextrin contained C, N, O, Au, Cl, etc. Further, C, N, and O came from PANi and beta-cyclodextrin; Cl was derived from the Au precursor (chloroauric acid). The contents of C, N, O, Au, and Cl from a microdomain containing Au nanoparticle in PANi/Au nanocomposites containing beta-cyclodextrin are shown in the Table 2.

Table 2. EDS results of one microdomain containing Au nanoparticle in PANi/Au nanocomposite containing beta-cyclodextrin.

Element	C	N	O	Au	Cl, etc.	Total
Mass percent (%)	62.61	7.47	9.96	15.09	4.87	100
Atomic percent (%)	79.11	8.09	9.45	1.16	2.19	100

As shown in Table 2, the element with the highest content is C, which was derived from PANi and beta-cyclodextrin. Although the mass percent content of Au is relatively high (about 15.09 %), the atomic percent of Au is only 1.16 % due to the high molecular weight of Au. This illustrates that the Au/PANi nanocomposites functionalized with beta-cyclodextrin contained Au; as the matrix of Au/PANi nanocomposites functionalized with beta-cyclodextrin was still polymer, the Au nanoparticle only acted as a filler. As shown from TEM (Figure 5), Au/PANi nanocomposites functionalized with beta-cyclodextrin showed that regardless of the morphology of the core/shell structure or the nanoparticles dispersed in the polymer matrix, nanoparticles were separated by an organic layer containing polymer. This organic layer acted in a protective role, preventing the aggregation of Au nanoparticles and enhancing the stability of nanocomposites. However, the distance between Au nanoparticles heavily affected carrier transfer since beta-cyclodextrin as an organic spacer is an insulating material. If the content of beta-cyclodextrin is appropriate, photo-generated electrons can tunnel or hop onto the organic layer [121,122]. Otherwise, electrons are trapped by the organic layer. Some chemical groups, such as the OH⁻ group of beta-cyclodextrin, can capture the electrons injected into the organic layer, breaking electron delocalization by the localized state and cutting the channel of carrier transfer.

Figure 7 shows that the absorbance of Au/PANi nanocomposite functionalized with beta-cyclodextrin covered the whole region of visible light and NIR. The band edge was from about 900 nm to over 1000 nm depending on the content of Au nanoparticles. Therefore, Au/PANi nanocomposites functionalized with beta-cyclodextrin should have a crucial prerequisite for holding visible light activity and NIR activity. When light (hν) triggers the surface of the nanocomposite, the process is complex and includes absorbance, scattering, transmission, light emittance, energy dissipation by scattering effects, free electron/hole production, and so on. The selection of a good physical process heavily depends on the microstructure and interface tailoring of the nanocomposite. Nanomaterials with external stimuli responses are one of the trends in intelligent materials and devices. External stimuli generally include pH, temperature, electric field, magnetic field, and light. Visible light activity is vital for energy and environmental demands, while NIR activity is favorable for

biomedical and information areas. For biomedical applications, two wavelength windows are popular for accepting applications: 808 nm and 1064 nm. This study emphasizes photo-current responses to weak visible light and 808 nm NIR (10–200 mW). The results indicate that the Au/PANi nanocomposites functionalized with beta-cyclodextrin showed good photo-current switching behaviors to weak visible light and 808 nm NIR. Even after three years of storage, the photo-response of the sample still exhibited photo-current switching behavior. This illustrates that the Au/PANi nanocomposites functionalized with beta-cyclodextrin had good stability in water due to the Au nanoparticles being coated with an isolating layer. This stability is augmented by the core/shell structure of the nanocomposites. This shell layer acts in a protective role, preventing the aggregation of Au nanoparticles and also promoting the separation of electron/hole in the interface between Au and PANi due to the strong coupling of plasmon and exciton between Au and PANi. The presence of hydroxypropyl- β -cyclodextrin is another critical factor for the dispersion stability of nanocomposite. Its role is similar to that of surfactant in dispersing the Au/PANi organic/inorganic hybrid in water. After the nanocomposite samples had been stored for over five years at room temperature, we re-examined the activity of Au/PANi nanocomposites to weak visible light by determining their photoconductivity to visible light. The samples still exhibited photo responses to light. Representative results of nanocomposite samples that had been stored for over three years are shown in Figure 10.

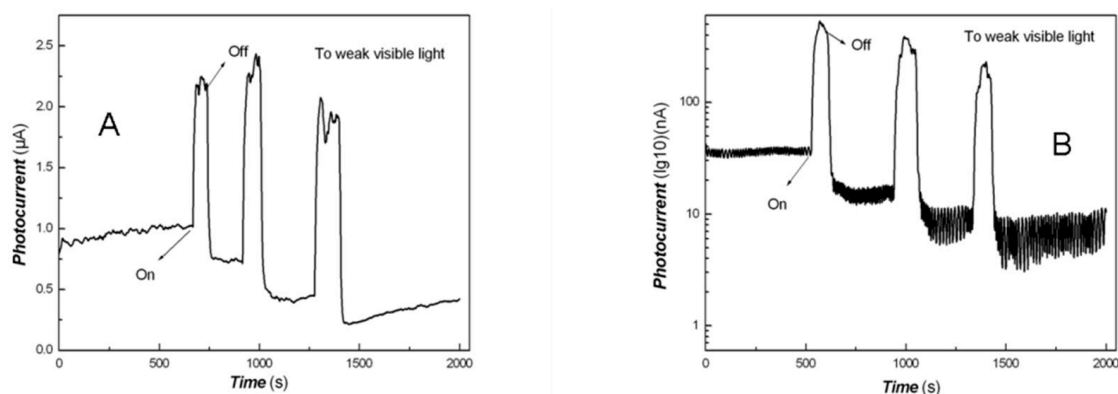


Figure 10. Photo-responses of Au/PANi nanocomposites functionalized with beta-cyclodextrin to weak visible light (A: Sample 2—chloroauric acid (50 mL); B: Sample 3—chloroauric acid (100 mL)).

The horizontal axis of Figure 10 is the response time (s). The vertical axis of Figure 8 is the value of the thick film current. As shown in Figure 8A,B, Au/PANi nanocomposites functionalized with beta-cyclodextrin still showed good photo-switching behaviors to weak visible light excitation. When the Au/PANi nanocomposites were exposed to visible light, the current of the film increased dramatically. On the contrary, the current of the film significantly decreased when the visible light was off. For PANi/beta-cyclodextrin/Au(50) nanomaterial thick film, the response time is approximately 33.42 s and the recovery time is approximately 11.15 s. Regarding PANi/beta-cyclodextrin/Au(100) nanomaterial thick film, the response time is approximately 50.56 s and the recovery time is approximately 16.29 s. Response and recovery are rapid to weak visible light. This also illustrates that the Au/PANi nanocomposites functionalized with beta-cyclodextrin produced photo-induced charges efficiently to weak visible light and possess good visible light activities. Therefore, free electron/hole were generated and separated with excitation of the low-power visible light sources. PANi/beta-cyclodextrin/Au nanocomposite's exhibition of photo-current switching behavior in the visible light region is mainly a result of surface plasmon resonance of Au nanoparticles. Under visible light irradiation, Au nanoparticles produced "hot electrons", and some of these electrons have sufficient energy to overcome the Schottky barrier (interface between Au and organic layer) and be injected into the LUMO level of PANi. The bandgap of PANi was narrowed (HOMO and LUMO energy level) [118–122]. Since PANi is a conjugated polymer, these carriers were transferred freely

in the PANi layer. The presence of beta-cyclodextrin in nanocomposite also produces interface barriers of Au/beta-cyclodextrin interface and PANi/beta-cyclodextrin interface for carrier transfer. Figure 10 also shows that the baseline current after exposure was lower than before exposure to visible light. This phenomenon was caused by photo-doping effects producing an in-built field. The direction of the in-built field is reversed to that of applied bias, and resulted in the decrease of current to some extent.

Visible light is considered to be in the range of 400–700 nm. Some representative wavelengths, such as 405 nm, 532 nm, and 650 nm, with low power (50 mW), were selected for further photo-excitation experiments. The representative results are shown in Figure 11.

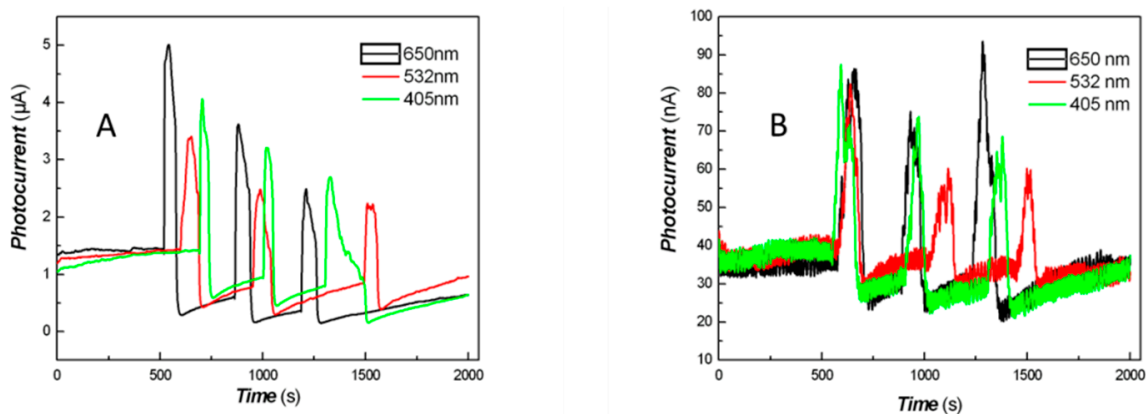


Figure 11. Photo-responses of Au/PANi nanocomposites functionalized with beta-cyclodextrin to 50 mW 405 nm, 532 nm, and 650 nm light (A: Sample 2-chloroauric acid (50 mL); B: Sample 3-chloroauric acid (100 mL)).

Figure 11 shows similar results between the Au/PANi nanocomposites functionalized with beta-cyclodextrin to 50 mW 405 nm, 532 nm, and 650 nm incident light (the vertical axis of Figure 9 is the film current). For PANi/beta-cyclodextrin/Au(50) nanomaterial thick film under 50 mW 405 nm, 532 nm, and 650 nm incident light, the response time is approximately 11.24 s, 43.09 s, and 15.93 s, respectively. The recovery time is approximately 22.48 s, 16.87 s, and 15.93 s. Regarding PANi/beta-cyclodextrin/Au(100) nanomaterial thick film under 50 mW 405 nm, 532 nm, and 650 nm incident light, the response time is approximately 32.79 s, 48.72 s, and 54.34 s, respectively. The recovery time is approximately 27.17 s, 22.49 s, and 32.80 s. Response and recovery are also rapid. The response rate of PANi/beta-cyclodextrin/Au(50) nanomaterial thick film is faster than that of PANi/beta-cyclodextrin/Au(100). The above results are only a preliminary examination, as whole free electron/hole pairs were easily generated and separated with excitation of 50 mW 405 nm, 532 nm, and 650 nm light resource for Au/PANi nanocomposite. Figure 11 also shows that the baseline current after exposure was lower than that before exposure. This phenomenon was caused by photo-doping effects producing an in-built field (as described previously). Another phenomenon is that the photo-current of the nanocomposite slowly decreased with extending exposure to light. This is the result of the imbalance between electrons injected into the organic layer and the detrapping process.

As shown from the UV-vis curve of Au/PANi nanocomposites, the Au/PANi nanocomposites functionalized with beta-cyclodextrin exhibited good absorbance in NIR. Therefore, 808 nm NIR at 100 mW was selected for studying the photoconductive response, due to 808 nm NIR having potential applications in the information and biomedical fields. The representative results are shown in Figure 12.

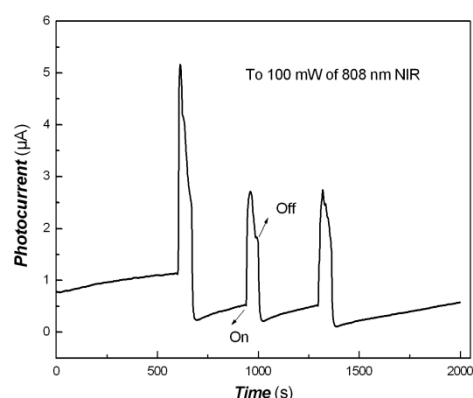


Figure 12. Photo-responses of Au/PANi nanocomposites functionalized with beta-cyclodextrin to 100 mW 808 nm NIR (Sample 2–chloroauric acid (50 mL)).

Figure 12 shows that the Au/PANi nanocomposites functionalized with beta-cyclodextrin exposed to 100 mW 808 nm NIR also exhibited good photo-current switching behavior (the vertical axis of Figure 10 is the film current). The response time is approximately 16.87 s, and recovery time is approximately 27.17s. These results are very exciting. It is well-known that Au nanoparticles generally have plasmon resonance properties in the range of the visible region. Enhancing surface plasmon resonance properties of Au nanomaterials in NIR requires synthesis of low-dimensional Au nanomaterials, which requires a large quantity of surfactants as soft templates and Ag⁺ as direction-controlling agents for the growth of low-dimensional Au, and the process is very complex and time-consuming. Although PANi has good absorbance in NIR, free electron/hole pairs are challenging to produce at excitation of weak light. The Au/PANi nanocomposites synthesized not only have good photoconductive response in visible light, but also show similar photocurrent response in NIR. This illustrates that strong interaction between Au and PANi was present; charge transfer between Au and PANi decreased the band gap of PANi (HOMO and LUMO energy level), as the photo-current of nanocomposite is caused by the energy level gap of PANi excitation. As shown from TEM of Au/PANi nanocomposites, this nanocomposite not only has core/shell-structured morphology, but also holds morphology of Au nanoparticles dispersed in the polymer matrix. Both morphologies exhibited good interface contacts between Au nanoparticles and organic layer. The strong coupling between PANi and Au nanoparticles promoted the charge separation to incident light exposure and decreased the power of excitation required. The effects of the power of incident light of 808 nm on the photocurrent responses are shown in Figure 13.

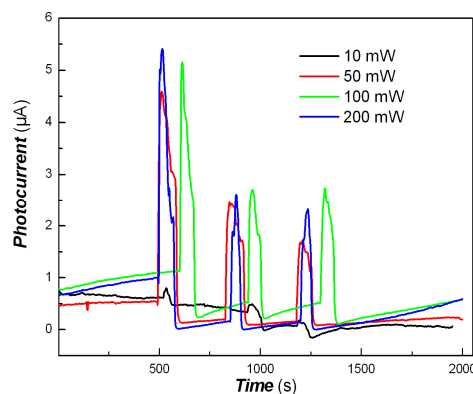


Figure 13. Photo-responses of Au/PANi nanocomposites functionalized with beta-cyclodextrin to 10, 50, 100, and 200 mW 808 nm NIR (Sample 2–chloroauric acid (50 mL)).

Figure 13 shows that the ratio of on/off was decreased clearly with reducing the power of incident light (the vertical axis of Figure 11 is the film current). There was still a slight

photocurrent response of Au/PANi nanocomposites functionalized with beta-cyclodextrin under 808 nm at 10 mW. The response time to 10, 50, 100, and 200 mW 808 nm NIR is approximately 21.71 s, 16.87 s, 17.14 s, and 6.27 s, respectively. The recovery time is approximately 43.42 s, 27.17 s, 11.14 s, and 7.32 s. This shows that the response rate and recovery rates are faster with increasing power of incident light.

To study the effects of different wavelengths of incident light on the photocurrent responses of Au/PANi nanocomposites, several representative wavelengths of incident light in NIR, such as 780 nm, 808 nm, 980 nm, and 1064 nm, were selected. The representative results are shown in Figure 14.

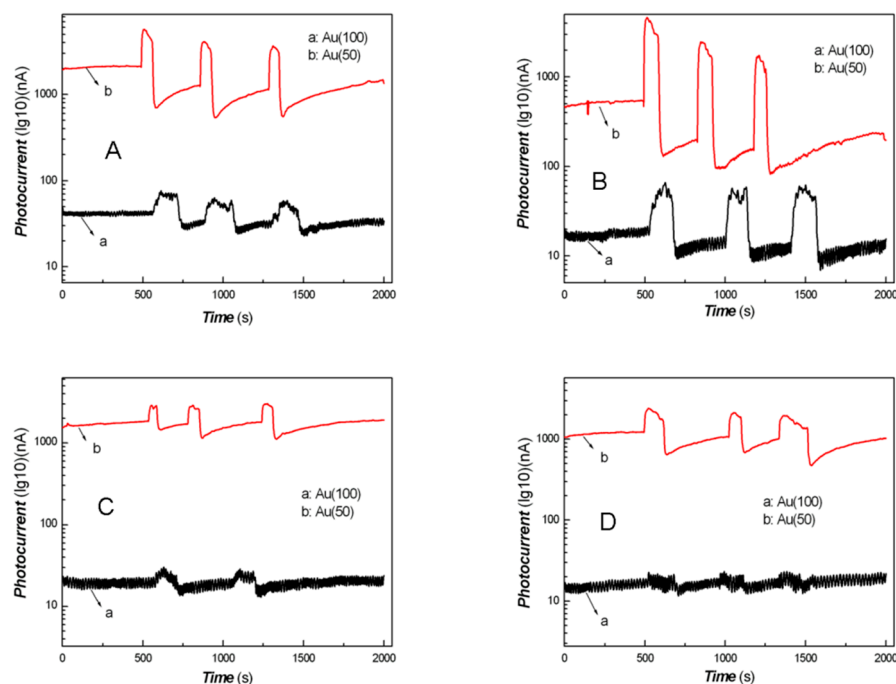


Figure 14. Photo-responses of Au/PANi nanocomposites functionalized with beta-cyclodextrin to 50 mW 780 nm, 808 nm, 980 nm and 1064 nm NIR. (A: 780 nm; B: 808 nm; C: 980 nm; D: 1064 nm) (a: Sample 3–chloroauric acid (100 mL); b: Sample 2–chloroauric acid (50 mL)).

Figure 14 shows that the Au/PANi nanocomposites functionalized with beta-cyclodextrin under 50 mW 780 nm, 808 nm, 980 nm, and 1064 nm NIR exhibited good photoconductivity responses at different ratios of on/off (the vertical axis of Figure 12 is the logarithm of film current (Lg[I])). The ratio of on/off to 808 nm NIR is much higher than that of other wavelengths. The photocurrent responses to 980 nm and 1064 nm are almost similar. For PANi/beta-cyclodextrin/Au(50) nanomaterial thick film under 50 mW 780 nm, 808 nm, 980 nm, and 1064 nm NIR, the response time is approximately 15.93 s, 16.87 s, 21.55 s, and 22.48 s, respectively. The recovery time is approximately 10.31 s, 27.17 s, 5.63 s, and 15.93 s, respectively. Regarding PANi/beta-cyclodextrin/Au(100) nanomaterial thick film under 50 mW 780 nm, 808 nm, 980 nm, and 1064 nm NIR, the response time is approximately 43.10 s, 71.21 s, 21.55 s, and 11.24 s, respectively. The recovery time is approximately 32.80 s, 21.55 s, 21.55 s, and 27.17 s, respectively. Response and recovery are also rapid. As shown in Figure 12, the photo-current switching ratio of PANi/beta-cyclodextrin/Au(50) nanomaterial thick film is higher than that of PANi/beta-cyclodextrin/Au(100). This illustrates that the gap distance between Au nanoparticles also affected the photo-current switching ratio because the surface plasmon resonance of Au nanoparticles depends on gap distance. Interestingly, the Au/PANi nanocomposites functionalized with beta-cyclodextrin to 1064 nm NIR of 50 mW still showed a good photo-current response. NIR at 1064 nm has promising applications in bio-imaging, information fields, etc. Another exciting result is that the photosensitivity of nanocomposites was decreased with the increasing content of Au nanoparticles. This illustrated that the surface

plasmon resonance of Au nanoparticles heavily depends on gap distance, and the strong interaction between PANi and Au nanoparticles promoted the separation of charges induced with incident light since the Au nanoparticles have good absorbance in the range of visible light (523 nm or so) due to surface plasmon resonance. To improve the optical properties in NIR of Au nanomaterials, low-dimensional controlled Au growth is often used. Therefore, this study provided a simple method to synthesize Au/PANi nanocomposite with good activity in NIR. This is promising for application in light detectors, photo-current switching, electrophotography, NIR-driven nano-carriers, photo-remote nanocomposites, information storage, bioimaging, etc.

For nearly 20 years, Ma and his coauthors have been very interested in organic/inorganic functional nanocomposites and their properties. The materials involved have included metal oxides, metal sulfides, carbon nanomaterials, conjugated polymers, non-conjugated polymers, conjugated organic small molecules, organic/inorganic hybrid nanostructures, and heterostructures [56,146–148]. Some exhibited good photo-current switching behaviors from the visible light region to NIR by tailoring interface engineering and defect engineering. The transfer of photo-generated carriers depends on the different interfaces for nanocomposites; the relationship between the interface of metal nanostructure/conjugated polymers/non-conjugated small organic molecules and photo-electric properties was the focus of this paper. Other material systems also show similar and unique responses.

4. Conclusions

In summary, Au/PANi nanocomposites containing beta-cyclodextrin were prepared by an interface polymerization approach. The nanocomposites exhibited good photo-current responses to weak visible light and low-power NIR, leading to many potential applications, such as light-sensitive nanocomposites, photo-current switches, photo-detectors, and information storage. The effects of different wavelengths and the power of incident light on the photocurrent responses of nanocomposites are clear. The Au/PANi nanocomposite's good activity in NIR was mainly attributed to the strong interaction between PANi and Au nanoparticles, promoting the charge separation of the interface of PANi/Au nanoparticles. Meanwhile, the resulting nanocomposites have good film-forming properties and long-term dispersing stability in water, which allows their use solution-processing technology for different applications. Therefore, this study provided a simple approach to preparing multi-functional organic/inorganic nanocomposites for broadband spectrum light-driven properties.

Author Contributions: X.M. conceived and designed the experiments; M.G. (FTIR, UV-Vis), C.L. (FTIR, XRD), X.Z. (XRD) and X.M. performed the experiments; all authors analyzed the data; X.M., wrote the paper; G.L. checked the English; all authors discussed the results. All authors have read and agreed to the published version of the manuscript.

Funding: This project had ever been supported by the Natural Science Foundation of Shandong Province (project No. ZR2013EMM008). Special Thanks to the State Key Laboratory of Industrial Control Technology and the State Key Lab of Silicon Materials, Zhejiang University. Thanks are also due to other graduating students (Bo Zhang and Qin Cong) who assisted with experiments. SEM and EDS were carried out by Wenhai Wang, Analysis and Measurement Center, Yantai Institute of Coastal Zone Research, Chinese Academy of Sciences. TEM was performed by Chunsheng Wang, Structural Composition Testing Center, School of Chemistry and Chemical Engineering, Shandong University.

Institutional Review Board Statement: Not applicable.

Informed Consent Statement: Not applicable.

Data Availability Statement: Data sharing is not applicable to this article.

Conflicts of Interest: We declare that we have no conflict of interest.

References

1. Alkuam, E.; Mohammed, M.; Chen, T. Fabrication of CdS nanorods and nanoparticles with PANI for (DSSCs) dye-sensitized solar cells. *Sol. Energy* **2017**, *150*, 317–324. [[CrossRef](#)]
2. He, B.; Tang, Q.; Wang, M.; Chen, H.; Yuan, S. Robust Polyaniline–Graphene Complex Counter Electrodes for Efficient Dye-Sensitized Solar Cells. *ACS Appl. Mater. Interfaces* **2014**, *6*, 8230–8236. [[CrossRef](#)] [[PubMed](#)]
3. Song, R.; Yan, K.; Lin, Z.; Loo, J.S.C.; Pan, L.; Zhang, Q.; Zhang, J.; Zhu, J. Inkjet-printed porous polyaniline gel as an efficient anode for microbial fuel cells. *J. Mater. Chem. A* **2016**, *4*, 14555–14559. [[CrossRef](#)]
4. Wu, R.; Tsai, M.; Ho, K.; Wei, T.; Hsieh, T.; Han, Y.; Kuo, C.; Tseng, P.; Wang, Y. Sulfonated polyaniline nanofiber as Pt-catalyst conducting support for proton exchange membrane fuel cell. *Polymer* **2014**, *55*, 2035–2043. [[CrossRef](#)]
5. Hursa'n, D.; Korma'nyos, A.; Rajeshwar, K.; Jana'ky, C. Polyaniline films photoelectrochemically reduce CO₂ to alcohols. *Chem. Commun.* **2016**, *52*, 8858–8861. [[CrossRef](#)]
6. Jeon, J.; Kwon, S.R.; Lutkenhaus, J.L. Polyaniline nanofiber/electrochemically reduced graphene oxide layer-by-layer electrodes for electrochemical energy storage. *J. Mater. Chem. A* **2015**, *3*, 3757–3767. [[CrossRef](#)]
7. Ge, D.; Yang, L.; Honglawan, A.; Li, J.; Yang, S. In Situ Synthesis of Hybrid Aerogels from Single-Walled Carbon Nanotubes and Polyaniline Nanoribbons as Free-Standing, Flexible Energy Storage Electrodes. *Chem. Mater.* **2014**, *26*, 1678–1685. [[CrossRef](#)]
8. Ramphal, I.A.; Hagerman, M.E. Water-Processable Laponite/Polyaniline/Graphene Oxide Nanocomposites for Energy Applications. *Langmuir* **2015**, *31*, 1505–1515. [[CrossRef](#)]
9. Wang, G.; Peng, J.; Zhang, L.; Zhang, J.; Dai, B.; Zhu, M.; Xia, L.; Yu, F. Two-dimensional SnS₂@PANI nanoplates with high capacity and excellent stability for lithium-ion batteries. *J. Mater. Chem. A* **2015**, *3*, 3659–3666. [[CrossRef](#)]
10. Dong, Y.; Zhao, Z.; Wang, Z.; Liu, Y.; Wang, X.; Qiu, J. Dually Fixed SnO₂ Nanoparticles on Graphene Nanosheets by Polyaniline Coating for Superior Lithium Storage. *ACS Appl. Mater. Interfaces* **2015**, *7*, 2444–2451. [[CrossRef](#)]
11. Lin, N.; Zhou, J.; Wang, L.; Zhu, Y.; Qian, Y. Polyaniline-Assisted Synthesis of Si@C/RGO as Anode Material for Rechargeable Lithium-Ion Batteries. *ACS Appl. Mater. Interfaces* **2015**, *7*, 409–414. [[CrossRef](#)] [[PubMed](#)]
12. Htut, K.Z.; Kim, M.; Lee, E.; Lee, G.; Baek, S.H.; Shim, S.E. Biodegradable polymer-modified graphene/polyaniline electrodes for supercapacitors. *Synth. Met.* **2017**, *227*, 61–70. [[CrossRef](#)]
13. Gu, D.; Ding, C.; Qin, Y.; Jiang, H.; Wang, L.; Shen, L. Behavior of electrical charge storage/release in polyaniline electrodes of symmetric supercapacitor. *Electrochim. Acta* **2017**, *245*, 146–155. [[CrossRef](#)]
14. Chang, C.; Hu, Z.; Lee, T.; Huang, Y.; Ji, W.; Liu, W.; Yeh, J.; Wei, Y. Biotemplated hierarchical polyaniline composite electrodes with high performance for flexible supercapacitors. *J. Mater. Chem. A* **2016**, *4*, 9133–9145.
15. Liu, Q.; Jing, S.; Wang, S.; Zhuo, H.; Zhong, L.; Peng, X.; Sun, R. Flexible nanocomposites with ultrahigh specific areal capacitance and tunable properties based on a cellulose derived nanofiber-carbon sheet framework coated with polyaniline. *J. Mater. Chem. A* **2016**, *4*, 13352–13362. [[CrossRef](#)]
16. Chao, J.; Deng, J.; Zhou, W.; Liu, J.; Hu, R.; Yang, L.; Zhu, M.; Schmidt, O.G. Hierarchical nanoflowers assembled from MoS₂/polyaniline sandwiched nanosheets for high-performance supercapacitors. *Electrochim. Acta* **2017**, *243*, 98–104. [[CrossRef](#)]
17. Wang, K.; Wu, H.; Meng, Y.; Wei, Z. Conducting Polymer Nanowire Arrays for High Performance Supercapacitors. *Small* **2014**, *10*, 14–31. [[CrossRef](#)]
18. Liu, T.; Finn, L.; Yu, M.; Wang, H.; Zhai, T.; Lu, X.; Tong, Y.; Li, Y. Polyaniline and Polypyrrole Pseudocapacitor Electrodes with Excellent Cycling Stability. *Nano Lett.* **2014**, *14*, 2522–2527. [[CrossRef](#)]
19. Tian, Y.; Cong, S.; Su, W.; Chen, H.; Li, Q.; Geng, F.; Zhao, Z. Synergy of W₁₈O₄₉ and Polyaniline for Smart Supercapacitor Electrode Integrated with Energy Level Indicating Functionality. *Nano Lett.* **2014**, *14*, 2150–2156. [[CrossRef](#)]
20. Chen, X.; Lin, H.; Deng, J.; Zhang, Y.; Sun, X.; Chen, P.; Fang, X.; Zhang, Z.; Guan, G.; Peng, H. Electrochromic Fiber-Shaped Supercapacitors. *Adv. Mater.* **2014**, *26*, 8126–8132. [[CrossRef](#)]
21. Zhao, H.; Yang, J.; Lin, T.; Lü, Q.; Chen, G. Nanocomposites of Sulfonic Polyaniline Nanoarrays on Graphene Nanosheets with an Improved Supercapacitor Performance. *Chem. Eur. J.* **2015**, *21*, 682–690. [[CrossRef](#)] [[PubMed](#)]
22. Jiang, W.; Yu, D.; Zhang, Q.; Goh, K.; Wei, L.; Yong, Y.; Jiang, R.; Wei, J.; Chen, Y. Ternary Hybrids of Amorphous Nickel Hydroxide–Carbon Nanotube–Conducting Polymer for Supercapacitors with High Energy Density, Excellent Rate Capability, and Long Cycle Life. *Adv. Funct. Mater.* **2015**, *25*, 1063–1073. [[CrossRef](#)]
23. Yang, X.; Liu, Y.; Lei, H.; Li, B. An organic–inorganic broadband photodetector based on a single polyaniline nanowire doped with quantum dots. *Nanoscale* **2016**, *8*, 15529–15537. [[CrossRef](#)]
24. Barman, T.; Pal, A.R. Plasmonic Photosensitization of Polyaniline Prepared by a Novel Process for High-Performance Flexible Photodetector. *ACS Appl. Mater. Interfaces* **2015**, *7*, 2166–2170. [[CrossRef](#)] [[PubMed](#)]
25. Pham, T.; Lee, B.; Nguyen, V.N.; Dao, V. Novel photocatalytic activity of vanadium-doped tantalum nitride sensitized/protected by polyaniline for efficient visible light water splitting. *J. Catal.* **2017**, *352*, 13–21. [[CrossRef](#)]
26. Zhang, M.; Wang, X. Two dimensional conjugated polymers with enhanced optical absorption and charge separation for photocatalytic hydrogen evolution. *Energy Environ. Sci.* **2014**, *7*, 1902–1906. [[CrossRef](#)]
27. Lu, X.; Zhang, Z.; Li, H.; Sun, X.; Peng, H. Conjugated polymer composite artificial muscle with solvent-induced anisotropic mechanical actuation. *J. Mater. Chem. A* **2014**, *2*, 17272–17280. [[CrossRef](#)]
28. Shi, Y.; Ma, C.; Peng, L.; Yu, G. Conductive “Smart” Hybrid Hydrogels with PNIPAM and Nanostructured Conductive Polymers. *Adv. Funct. Mater.* **2015**, *25*, 1219–1225. [[CrossRef](#)]

29. Tian, Y.; Zhang, X.; Dou, S.; Zhang, L.; Zhang, H.; Lv, H.; Wang, L.; Zhao, J.; Li, Y. A comprehensive study of electrochromic device with variable infrared emissivity based on polyaniline conducting polymer. *Sol. Energy Mater. Sol. Cells* **2017**, *170*, 120–126. [[CrossRef](#)]
30. Zhu, X.; Zhao, J.; Wang, C. Acid and base dual-controlled cargo molecule release from polyaniline gated-hollow mesoporous silica nanoparticles. *Polym. Chem.* **2016**, *7*, 6467–6474. [[CrossRef](#)]
31. Gong, X.; Fei, G.; Fu, W.; Fang, M.; Gao, X.; Zhong, B.; Zhang, L. Flexible strain sensor with high performance based on PANI/PDMS films. *Org. Electron.* **2017**, *47*, 51–56. [[CrossRef](#)]
32. Lee, B.H.; Lee, J.; Kahng, Y.H.; Kim, N.; Kim, Y.J.; Lee, J.; Lee, T.; Lee, K. Graphene-Conducting Polymer Hybrid Transparent Electrodes for Efficient Organic Optoelectronic Devices. *Adv. Funct. Mater.* **2014**, *24*, 1847–1856. [[CrossRef](#)]
33. Meng, D.; Yang, S.; Guo, L.; Li, G.; Ge, J.; Huang, Y.; Bielawski, C.W.; Geng, J. The enhanced photothermal effect of graphene/conjugated polymer composites: Photoinduced energy transfer and applications in photocontrolled switches. *Chem. Commun.* **2014**, *50*, 14345–14348. [[CrossRef](#)] [[PubMed](#)]
34. Li, J.; Liu, L.; Zhang, D.; Yang, D.; Guo, J.; Wei, J. Fabrication of polyaniline/silver nanoparticles/multi-walled carbonnanotubes composites for flexible microelectronic circuits. *Synth. Met.* **2014**, *192*, 15–22. [[CrossRef](#)]
35. Jiang, N.; Shao, L.; Wang, J. (Gold Nanorod Core)/(Polyaniline Shell) Plasmonic Switches with Large Plasmon Shifts and Modulation Depths. *Adv. Mater.* **2014**, *26*, 3282–3289. [[CrossRef](#)]
36. Ramana, G.V.; Srikanth, V.V.S.S.; Padya, B.; Jain, P.K. Carbon nanotube–polyaniline nanotube core–shell structures for electrochemical applications. *Eur. Polym. J.* **2014**, *57*, 137–142. [[CrossRef](#)]
37. Guo, Y.; Wang, T.; Chen, F.; Sun, X.; Li, X.; Yu, Z.; Wan, P.; Chen, X. Hierarchical graphene–polyaniline nanocomposite films for high-performance flexible electronic gas sensors. *Nanoscale* **2016**, *8*, 12073–12080. [[CrossRef](#)]
38. Rao, H.; Chen, M.; Ge, H.; Lu, Z.; Liu, X.; Zou, P.; Wang, X.; He, H.; Zeng, X.; Wang, Y. A novel electrochemical sensor based on Au@PANI composites film modified glassy carbon electrode binding molecular imprinting technique for the determination of melamine. *Biosens. Bioelectron.* **2017**, *87*, 1029–1035. [[CrossRef](#)]
39. Wang, W.; Xu, G.; Cui, X.T.; Sheng, G.; Luo, X. Enhanced catalytic and dopamine sensing properties of electrochemically reduced conducting polymer nanocomposite doped with pure graphene oxide. *Biosens. Bioelectron.* **2014**, *58*, 153–156. [[CrossRef](#)]
40. Rana, U.; Paul, N.D.; Mondal, S.; Chakraborty, C.; Malik, S. Water soluble polyaniline coated electrode: A simple and nimble electrochemical approach for ascorbic acid detection. *Synth. Met.* **2014**, *192*, 43–49. [[CrossRef](#)]
41. Yang, T.; Yang, R.; Chen, H.; Nan, F.; Ge, T.; Jiao, K. Electrocatalytic Activity of Molybdenum Disulfide Nanosheets Enhanced by Self-Doped Polyaniline for Highly Sensitive and Synergistic Determination of Adenine and Guanine. *ACS Appl. Mater. Interfaces* **2015**, *7*, 2867–2872. [[CrossRef](#)] [[PubMed](#)]
42. Andreyev, E.A.; Komkova, M.A.; Nikitina, V.N.; Zaryanov, N.V.; Voronin, O.G.; Karyakina, E.E.; Yatsimirsky, A.K.; Karyakin, A.A. Reagentless Polyol Detection by Conductivity Increase in the Course of Self-Doping of Boronate-Substituted Polyaniline. *Anal. Chem.* **2014**, *86*, 11690–11695. [[CrossRef](#)] [[PubMed](#)]
43. Zhang, L.; Zhou, C.; Luo, J.; Long, Y.; Wang, C.; Yu, T.; Xiao, D. A polyaniline microtube platform for direct electron transfer of glucose oxidase and biosensing applications. *J. Mater. Chem. B* **2015**, *3*, 1116–1124. [[CrossRef](#)] [[PubMed](#)]
44. Radoi´ci´c, M.; Ciri´c-Marjanovi´c, G.; Spasojevi´c, V.; Ahrenkiel, P.; Mitri´ca, M.; Novakovi´cd, T.; Saponji´ca, Z. Superior photocatalytic properties of carbonized PANI/TiO₂ nanocomposites. *Appl. Catal. B Environ.* **2017**, *213*, 155–166. [[CrossRef](#)]
45. Liu, Z.; Miao, Y.; Liu, M.; Ding, Q.; Tjiu, W.W.; Cui, X.; Liu, T. Flexible polyaniline-coated TiO₂/SiO₂ nanofiber membranes with enhanced visible-light photocatalytic degradation performance. *J. Colloid Interface Sci.* **2014**, *424*, 49–55. [[CrossRef](#)]
46. Bogdanovi´c, U.; Vodnik, V.; Mitri´c, M.; Dimitrijevi´c, S.; Škapin, S.D.; Žuni´c, V.; Budimir, M.; Stoiljkovi´c, M. Nanomaterial with High Antimicrobial Efficacy of Copper/Polyaniline Nanocomposite. *ACS Appl. Mater. Interfaces* **2015**, *7*, 1955–1966. [[CrossRef](#)]
47. Poyraz, S.; Cerkez, I.; Huang, T.S.; Liu, Z.; Kang, L.; Luo, J.; Zhang, X. One-Step Synthesis and Characterization of Polyaniline Nanofiber/Silver Nanoparticle Composite Networks as Antibacterial Agents. *ACS Appl. Mater. Interfaces* **2014**, *6*, 20025–20034. [[CrossRef](#)]
48. Zhang, X.; Goux, W.J.; Manohar, S.K. Synthesis of polyaniline nanofibers by “Nanofiber Seeding”. *J. Am. Chem. Soc.* **2004**, *126*, 4502–4503. [[CrossRef](#)]
49. Huang, J.; Kaner, R.B. Nanofiber formation in the chemical polymerization of aniline: A mechanistic study. *Angew. Chem. Int. Ed.* **2004**, *43*, 5817–5821. [[CrossRef](#)]
50. Li, C.; Bai, H.; Shi, G. Conducting polymer nanomaterials: Electro-synthesis and applications. *Chem Soc. Rev.* **2009**, *38*, 2397–2409. [[CrossRef](#)]
51. Ma, Y.; Zhang, J.; Zhang, G.; He, H. Polyaniline nanowires on Si surfaces fabricated with DNA templates. *J. Am. Chem. Soc.* **2004**, *126*, 7097–7101. [[CrossRef](#)] [[PubMed](#)]
52. Huang, J.; Virji, S.; Weiller, B.H.; Kaner, R.B. Polyaniline nanofibers: Facile synthesis and chemical sensors. *J. Am. Chem. Soc.* **2003**, *125*, 314–315. [[CrossRef](#)] [[PubMed](#)]
53. Virji, S.; Huang, J.; Kaner, R.B.; Weiller, B.H. Polyaniline nanofiber gas sensors: Examination of response mechanisms. *Nano Lett.* **2004**, *4*, 491–496. [[CrossRef](#)]
54. Huang, J.; Virji, S.; Weiller, B.H.; Kaner, R.B. Nanostructure polyaniline sensors. *Chem. Eur. J.* **2004**, *10*, 1314–1319. [[CrossRef](#)] [[PubMed](#)]

55. Ma, X.; Li, G.; Wang, M.; Cheng, Y.; Bai, R.; Chen, H. Preparation of Nano-wire Structured Polyaniline Composite and its Gas-sensitivity Studies. *Chem. A Eur. J.* **2006**, *12*, 3254–3260. [[CrossRef](#)]
56. Ma, X.; Wang, M.; Li, G.; Chen, H.; Bai, R. Preparation of Polyaniline-TiO₂ Composite Film with in-situ Polymerization Approach and Its Gas-sensitivity at Room Temperature. *Mater. Chem. Phys.* **2006**, *98*, 241–247. [[CrossRef](#)]
57. Ma, X.; Gao, M.; He, X.; Li, G. Morphology Tailoring of Nano/Micro-structured Conductive Polymers, Composites and Their Applications in Chemical Sensors. *Recent Pat. Nanotechnol.* **2010**, *4*, 150–163. [[CrossRef](#)]
58. Ma, X.; Wang, M.; Chen, H.; Li, G.; Sun, J.; Bai, R. Preparation of Water Soluble Poly (aniline) and its Gas-sensitivity. *Green Chem.* **2005**, *7*, 507–513. [[CrossRef](#)]
59. Ma, X.; Li, G.; Wang, M.; Bai, R.; Yang, F.; Chen, H. Unusual Electrical Response of Poly(aniline) Composite Film on Exposure to the Atmosphere of Base and its Applications on Sensors. *Green Chem.* **2006**, *8*, 63–69. [[CrossRef](#)]
60. Xu, S.; Gao, T.; Feng, X.; Fan, X.; Liu, G.; Mao, Y.; Yu, X.; Lin, J.; Luo, X. Near infrared fluorescent dual ligand functionalized Au NCs based multidimensional sensor array for pattern recognition of multiple proteins and serum discrimination. *Biosens. Bioelectron.* **2017**, *97*, 203–207. [[CrossRef](#)]
61. Huang, Q.; Lin, X.; Zhu, J.; Tong, Q. Pd-Au@carbon dots nanocomposite: Facile synthesis and application as an ultrasensitive electrochemical biosensor for determination of colitoxin DNA in human serum. *Biosens. Bioelectron.* **2017**, *94*, 507–512. [[CrossRef](#)] [[PubMed](#)]
62. Zhang, H.; Zhang, L.; Han, Y.; Yu, Y.; Xu, M.; Zhang, X.; Huang, L.; Dong, S. RGO/Au NPs/N-doped CNTs supported on nickel foam as an anode for enzymatic biofuel cells. *Biosens. Bioelectron.* **2017**, *97*, 34–40. [[CrossRef](#)] [[PubMed](#)]
63. Amoli-Diva, M.; Sadighi-Bonabi, R.; Pourghazi, K. Switchable on/off drug release from gold nanoparticles-grafted dual light- and temperature-responsive hydrogel for controlled drug delivery. *Mater. Sci. Eng. C* **2017**, *76*, 242–248. [[CrossRef](#)]
64. Wei, Y.; Li, X.; Sun, X.; Ma, H.; Zhang, Y.; Wei, Q. Dual-responsive electrochemical immunosensor for prostate specific antigen detection based on Au-CoS/graphene and CeO₂/ionic liquids doped with carboxymethyl chitosan complex. *Biosens. Bioelectron.* **2017**, *94*, 141–147. [[CrossRef](#)] [[PubMed](#)]
65. Liu, C.; Tai, H.; Zhang, P.; Ye, Z.; Su, Y.; Jiang, Y. Enhanced ammonia-sensing properties of PANI-TiO₂-Au ternary self-assembly nanocomposite thin film at room temperature. *Sens. Actuators B* **2017**, *246*, 85–95. [[CrossRef](#)]
66. Schmidt, I.; Gad, A.; Scholz, G.; Boht, H.; Martens, M.; Schilling, M.; Wasisto, H.S.; Waag, A.; Schröder, U. Gold-modified indium tin oxide as a transparent window in optoelectronic diagnostics of electrochemically active biofilms. *Biosens. Bioelectron.* **2017**, *94*, 74–80. [[CrossRef](#)] [[PubMed](#)]
67. Zhao, Y.; Li, X.; Liu, Y.; Zhang, L.; Wang, F.; Lu, Y. High performance surface-enhanced Raman scattering sensing based on Au nanoparticle-monolayer graphene-Ag nanostar array hybrid system. *Sens. Actuators B* **2017**, *247*, 850–857. [[CrossRef](#)]
68. Gole, A.; Murphy, C.J. Seed-Mediated Synthesis of Gold Nanorods: Role of the Size and Nature of the Seed. *Chem. Mater.* **2004**, *16*, 3633–3640. [[CrossRef](#)]
69. Placido, T.; Comparelli, R.; Giannici, F.; Cozzoli, P.D.; Capitani, G.; Striccoli, M.; Agostiano, A.; Curri, M.L. Photochemical Synthesis of Water-Soluble Gold Nanorods: The Role of Silver in Assisting Anisotropic Growth. *Chem. Mater.* **2009**, *21*, 4192–4202. [[CrossRef](#)]
70. Park, K.; Drummy, L.F.; Wadams, R.C.; Koerner, H.; Nepal, D.; Fabris, L.; Vaia, R.A. Growth Mechanism of Gold Nanorods. *Chem. Mater.* **2013**, *25*, 555–563. [[CrossRef](#)]
71. Fazal, S.; Jayasree, A.; Sasidharan, S.; Koyakutty, M.; Nair, S.V.; Menon, D. Green Synthesis of Anisotropic Gold Nanoparticles for Photothermal Therapy of Cancer. *ACS Appl. Mater. Interfaces* **2014**, *6*, 8080–8089. [[CrossRef](#)] [[PubMed](#)]
72. Chen, J.; Cao, S.; Xi, C.; Chen, Y.; Li, X.; Zhang, L.; Wang, G.; Chen, Y.; Chen, Z. A novel magnetic β -cyclodextrin modified graphene oxide adsorbent with high recognition capability for 5 plant growth regulators. *Food Chem.* **2018**, *239*, 911–919. [[CrossRef](#)] [[PubMed](#)]
73. Zaidi, S.A. Facile and efficient electrochemical enantiomer recognition of phenylalanine using β -Cyclodextrin immobilized on reduced graphene oxide. *Biosens. Bioelectron.* **2017**, *94*, 714–718. [[CrossRef](#)] [[PubMed](#)]
74. Shi, P.; Liu, Z.; Dong, K.; Ju, E.; Ren, J.; Du, Y.; Li, Z.; Qu, X. A Smart “Sense-Act-Treat” System: Combining a Ratiometric pH Sensor with a Near Infrared Therapeutic Gold Nanocage. *Adv. Mater.* **2014**, *26*, 6635–6641. [[CrossRef](#)]
75. Sen, T.; Mishra, S.; Shimpi, N.G. A β -cyclodextrin based binary dopant for polyaniline: Structural, thermal, electrical, and sensing performance. *Mater. Sci. Eng. B* **2017**, *220*, 13–21. [[CrossRef](#)]
76. Ma, M.; Zhe, T.; Song, W.; Guo, P.; Wang, J.; Wang, J. A comparative study on the glucose sensors modified by two different β -cyclodextrin functionalized reduced graphene oxide based Au nanocomposites synthesized through developed post immobilization and in situ growth technologies. *Sens. Actuators B* **2017**, *253*, 818–829. [[CrossRef](#)]
77. Chen, J.; He, P.; Bai, H.; He, S.; Zhang, T.; Zhang, X.; Dong, F. Poly (β -cyclodextrin)/carbon quantum dots modified glassy carbon electrode: Preparation, characterization and simultaneous electrochemical determination of dopamine, uric acid and tryptophan. *Sens. Actuators B* **2017**, *252*, 9–16. [[CrossRef](#)]
78. Li, C.; Wu, Z.; Yang, H.; Deng, L.; Chen, X. Reduced graphene oxide-cyclodextrin-chitosan electrochemical sensor: Effective and simultaneous determination of o- and p-nitrophenols. *Sens. Actuators B* **2017**, *251*, 446–454. [[CrossRef](#)]
79. Luo, M.; Hua, Y.; Liang, Y.; Han, J.; Liu, D.; Zhao, W.; Wang, P. Synthesis of novel β -cyclodextrin functionalized S, N co-doped carbon dots for selective detection of testosterone. *Biosens. Bioelectron.* **2017**, *98*, 195–201. [[CrossRef](#)]

80. Sedghi, R.; Heidari, B.; Yassari, M. Novel molecularly imprinted polymer based on β -cyclodextrin@graphene oxide: Synthesis and application for selective diphenylamine determination. *J. Colloid Interface Sci.* **2017**, *503*, 47–56. [[CrossRef](#)]
81. Peng, L.; Ye, L.; Cao, J.; Chang, Y.; Li, Q.; An, M.; Tan, Z.; Xu, J. Cyclodextrin-based miniaturized solid phase extraction for biopesticides analysis in water and vegetable juices samples analyzed by ultra-high-performance liquid chromatography coupled with quadrupole time-of-flight mass spectrometry. *Food Chem.* **2017**, *226*, 141–148. [[CrossRef](#)] [[PubMed](#)]
82. Zhang, W.; Lin, M.; Wang, M.; Tong, P.; Lu, Q.; Zhang, L. Magnetic porous β -cyclodextrin polymer for magnetic solid-phase extraction of microcystins from environmental water samples. *J. Chromatogr. A* **2017**, *1503*, 1–11. [[CrossRef](#)] [[PubMed](#)]
83. Zheng, H.; Ma, J.; Feng, W.; Jia, Q. Specific enrichment of glycoproteins with polymer monolith functionalized with glycocluster grafted β -cyclodextrin. *J. Chromatogr. A* **2017**, *1512*, 88–97. [[CrossRef](#)] [[PubMed](#)]
84. Skorb, E.V.; Möhwald, H. “Smart” Surface Capsules for Delivery Devices. *Adv. Mater. Interfaces* **2014**, *1*, 1400237. [[CrossRef](#)]
85. Hu, Q.; Tang, G.; Chu, P.K. Cyclodextrin-Based Host–Guest Supramolecular Nanoparticles for Delivery: From Design to Applications. *Acc. Chem. Res.* **2014**, *47*, 2017–2025. [[CrossRef](#)]
86. Kettel, M.J.; Schaefer, K.; Groll, J.; Moeller, M. Nanogels with High Active β -Cyclodextrin Content as Physical Coating System with Sustained Release Properties. *ACS Appl. Mater. Interfaces* **2014**, *6*, 2300–2311. [[CrossRef](#)]
87. Constantin, M.; Bucatariu, S.; Ascenzi, P.; Simionescu, B.C. Gheorghe Fundueanu, Poly (NIPAAm-co- β -cyclodextrin) microgels with drug hosting and temperature-dependent delivery properties. *React. Funct. Polym.* **2014**, *84*, 1–9. [[CrossRef](#)]
88. Li, R.Q.; Niu, Y.L.; Zhao, N.N.; Yu, B.R.; Mao, C.; Xu, F.J. Series of New β -Cyclodextrin-Cored Star-like Carriers for Gene Delivery. *ACS Appl. Mater. Interfaces* **2014**, *6*, 3969–3978. [[CrossRef](#)]
89. Kong, L.; Zhang, F.; Xing, P.; Chu, X.; Hao, A. A binary solvent gel as drug delivery carrier. *Colloids Surf. A Physicochem. Eng. Asp.* **2017**, *522*, 577–584. [[CrossRef](#)]
90. Xiong, Q.; Cui, M.; Bai, Y.; Liu, Y.; Liu, D.; Song, T. A supramolecular nanoparticle system based on β -cyclodextrin-conjugated poly-l-lysine and hyaluronic acid for co-delivery of gene and chemotherapy agent targeting hepatocellular carcinoma. *Colloids Surf. B Biointerfaces* **2017**, *155*, 93–103. [[CrossRef](#)]
91. Varan, G.; Varan, C.; Erdoğan, N.; Hincal, A.A.; Bilensoy, E. Amphiphilic cyclodextrin nanoparticles. *Int. J. Pharm.* **2017**, *531*, 457–469. [[CrossRef](#)] [[PubMed](#)]
92. Song, M.; Li, L.; Zhang, Y.; Chen, K.; Wang, H.; Gong, R. Carboxymethyl- β -cyclodextrin grafted chitosan nanoparticles as oral delivery carrier of protein drugs. *React. Funct. Polym.* **2017**, *117*, 10–15. [[CrossRef](#)]
93. Krzak, A.; Swiech, O.; Majdecki, M.; Bilewicz, R. Complexing daunorubicin with β -cyclodextrin derivative increases drug intercalation into DNA. *Electrochim. Acta* **2017**, *247*, 139–148. [[CrossRef](#)]
94. Adeoye, O.; Cabral-Marques, H. Cyclodextrin nanosystems in oral drug delivery: A mini review. *Int. J. Pharm.* **2017**, *531*, 521–531. [[CrossRef](#)] [[PubMed](#)]
95. Li, X.; Guo, T.; Lachmanski, L.; Manoli, F.; Menendez-Miranda, M.; Manet, I.; Guo, Z.; Wu, L.; Zhang, J.; Gref, R. Cyclodextrin-based metal-organic frameworks particles as efficient carriers for lansoprazole: Study of morphology and chemical composition of individual particles. *Int. J. Pharm.* **2017**, *531*, 424–432. [[CrossRef](#)]
96. Salzano, G.; Wankar, J.; Ottani, S.; Villemagne, B.; Baulard, A.R.; Willand, N.; Brodin, P.; Manet, I.; Gref, R. Cyclodextrin-based nanocarriers containing a synergic drug combination: A potential formulation for pulmonary administration of antitubercular drugs. *Int. J. Pharm.* **2017**, *531*, 577–587. [[CrossRef](#)]
97. Coviello, V.; Sartini, S.; Quattrini, L.; Baraldi, C.; Gamberini, M.C.; Motta, C.L. Cyclodextrin-based nanosponges for the targeted delivery of the anti-restenotic agent DB103: A novel opportunity for the local therapy of vessels wall subjected to percutaneous intervention. *Eur. J. Pharm. Biopharm.* **2017**, *117*, 276–285. [[CrossRef](#)]
98. Stjern, L.; Voittoinen, S.; Weldemichel, R.; Thuresson, S.; Agnes, M.; Benkovics, G.; Fenyvesi, É.; Malanga, M.; Yannakopoulou, K.; Feiler, A.; et al. Cyclodextrin-mesoporous silica particle composites for controlled antibiotic release. A proof of concept toward colon targeting. *Int. J. Pharm.* **2017**, *531*, 595–605. [[CrossRef](#)]
99. Cutrone, G.; Casas-Solvas, J.M.; Vargas-Berenguel, A. Cyclodextrin-Modified Inorganic Materials for the Construction of Nanocarriers. *Int. J. Pharm.* **2017**, *531*, 621–639. [[CrossRef](#)]
100. d’Angelo, I.; Fraix, A.; Ungaro, F.; Quaglia, F.; Miro, A. Poly(ethylene oxide)/hydroxypropyl- β -cyclodextrin films for oromucosal delivery of hydrophilic drugs. *Int. J. Pharm.* **2017**, *531*, 606–613. [[CrossRef](#)]
101. Elezaby, R.S.; Gad, H.A.; Metwally, A.A.; Geneidi, A.S.; Awad, G.A. Self-assembled amphiphilic core-shell nanocarriers in line with the modern strategies for brain delivery. *J. Control. Release* **2017**, *261*, 43–61. [[CrossRef](#)] [[PubMed](#)]
102. Gao, Y.; Li, G.; Zhou, Z.; Gao, L.; Tao, Q. Sensitive complex micelles based on host-guest recognition from chitosan-graft- β -cyclodextrin for drug release. *Int. J. Biol. Macromol.* **2017**, *105*, 74–80. [[CrossRef](#)] [[PubMed](#)]
103. Ramasamy, T.; Ruttala, H.B.; Gupta, B.; Poudel, B.K.; Choi, H.; Yong, C.S.; Kim, J.O. Smart chemistry-based nanosized drug delivery systems for systemic applications: A comprehensive review. *J. Control. Release* **2017**, *258*, 226–253. [[CrossRef](#)] [[PubMed](#)]
104. Yi, P.; Wang, Y.; He, P.; Zhan, Y.; Sun, Z.; Li, Y.; Zhang, Y. Study on β -cyclodextrin-complexed nanogels with improved thermal response for anticancer drug delivery. *Mater. Sci. Eng. C* **2017**, *78*, 773–779. [[CrossRef](#)] [[PubMed](#)]
105. Topuz, F.; Uyar, T. Cyclodextrin-functionalized mesostructured silica nanoparticles for removal of polycyclic aromatic hydrocarbons. *J. Colloid Interface Sci.* **2017**, *497*, 233–241. [[CrossRef](#)]

106. Gupta, V.K.; Agarwal, S.; Sadegh, H.; Ali, G.A.M.; Bharti, A.K.; Makhlof, A.S.H. Facile route synthesis of novel graphene oxide- β -cyclodextrin nanocomposite and its application as adsorbent for removal of toxic bisphenol A from the aqueous phase. *J. Mol. Liq.* **2017**, *237*, 466–472. [[CrossRef](#)]
107. Tan, P.; Hu, Y. Improved synthesis of graphene/ β -cyclodextrin composite for highly efficient dye adsorption and removal. *J. Mol. Liq.* **2017**, *242*, 181–189. [[CrossRef](#)]
108. Liu, G.; Li, L.; Xu, D.; Huang, X.; Xu, X.; Zheng, S.; Zhang, Y.; Lin, H. Metal-organic framework preparation using magnetic graphene oxide- β -cyclodextrin for neonicotinoid pesticide adsorption and removal. *Carbohydr. Polym.* **2017**, *175*, 584–591. [[CrossRef](#)]
109. Ragavan, K.V.; Rastogi, N.K. β -Cyclodextrin capped graphene-magnetite nanocomposite for selective adsorption of Bisphenol-A. *Carbohydr. Polym.* **2017**, *168*, 129–137. [[CrossRef](#)]
110. Parsamanesh, M.; Tehrani, A.D.; Mansourpanah, Y. Supramolecular hydrogel based on cyclodextrin modified GO as a potent natural organic matter absorbent. *Eur. Polym. J.* **2017**, *92*, 126–136. [[CrossRef](#)]
111. Tang, C.; Shiri, M.; Zhang, H.; Ayinla, R.T.; Wang, K. Light-Driven Charge Transport and Optical Sensing in Molecular Junctions. *Nanomaterials* **2022**, *12*, 698. [[CrossRef](#)] [[PubMed](#)]
112. Sendler, T.; Luka-Guth, K.; Wieser, M.; Wolf, J.; Helm, M.; Gemming, S.; Kerbusch, J.; Huhn, T.; Erbe, A. Light-Induced Switching of Tunable Single-Molecule Junctions. *Adv. Sci.* **2015**, *2*, 1500017. [[CrossRef](#)]
113. van der Molen, S.J.; Liljeroth, P. Charge transport through molecular switches. *J. Phys. Condens. Matter.* **2010**, *22*, 133001. [[CrossRef](#)] [[PubMed](#)]
114. Taherinia, D.; Frisbie, C.D. Photoswitchable Hopping Transport in Molecular Wires 4 nm in Length. *J. Phys. Chem. C* **2016**, *120*, 6442–6449. [[CrossRef](#)]
115. Yu, Z.; Xu, Y.; Su, J.; Radjenovic, P.M.; Wang, Y.; Zheng, J.; Teng, B.; Shao, Y.; Zhou, X.; Li, J. Probing Interfacial Electronic Effects on Single-Molecule Adsorption Geometry and Electron Transport at Atomically Flat Surfaces. *Angew. Chem. Int. Ed.* **2021**, *60*, 15452–15458. [[CrossRef](#)]
116. Jia, C.; Wang, J.; Yao, C.; Cao, Y.; Zhong, Y.; Liu, Z.; Liu, Z.; Guo, X. Conductance Switching and Mechanisms in Single-Molecule Junctions. *Angew. Chem. Int. Ed.* **2013**, *52*, 8666–8670. [[CrossRef](#)] [[PubMed](#)]
117. Huang, X.; Li, T. Recent progress in the development of molecular-scale electronics based on photoswitchable molecules. *J. Mater. Chem. C* **2020**, *8*, 821–848. [[CrossRef](#)]
118. Schwartz, T.; Hutchison, J.A.; Genet, C.; Ebbesen, T.W. Reversible Switching of Ultrastrong Light-Molecule Coupling. *Phys. Rev. Lett.* **2011**, *106*, 196405. [[CrossRef](#)]
119. Zhuang, M.; Ernzerhof, M. Mechanism of a molecular electronic photoswitch. *Phys. Rev. B* **2005**, *72*, 073104. [[CrossRef](#)]
120. Browne, W.R.; Feringa, B.L. Light Switching of Molecules on Surfaces. *Annu. Rev. Phys. Chem.* **2009**, *60*, 407–428. [[CrossRef](#)]
121. Choi, S.H.; Frisbie, C.D. Enhanced Hopping Conductivity in Low Band Gap Donor-Acceptor Molecular Wires Up to 20 nm in Length. *J. Am. Chem. Soc.* **2010**, *132*, 16191–16201. [[CrossRef](#)] [[PubMed](#)]
122. Choi, S.H.; Risko, C.; Delgado, M.C.R.; Kim, B.S.; Bre´das, J.; Frisbie, C.D. Transition from Tunneling to Hopping Transport in Long, Conjugated Oligo-imine Wires Connected to Metals. *J. Am. Chem. Soc.* **2010**, *132*, 4358–4368. [[CrossRef](#)]
123. Trindade, E.C.A.; Antˆonio, R.V.; Brandes, R.; de Souza, L.; Neto, G.; Vargas, V.M.M.; Carminatti, C.A.; Recouvreux, D.d.S. Carbon fiber-embedded bacterial cellulose/polyaniline nanocomposite with tailored for microbial fuel cells electrode. *J. Appl. Polym. Sci.* **2020**, *137*, 49036. [[CrossRef](#)]
124. Krishna, M.; Ghosh, A.; Muthuraj, D.; Das, S.; Mitra, S. Electrocatalytic Activity of Polyaniline in Magnesium–Sulfur Batteries. *J. Phys. Chem. Lett.* **2022**, *13*, 1337–1343. [[CrossRef](#)] [[PubMed](#)]
125. Almtiri, M.; Dowell, T.J.; Giri, H.; Wipf, D.O.; Scott, C.N. Electrochemically Stable Carbazole-Derived Polyaniline for Pseudocapacitors. *ACS Appl. Polym. Mater.* **2022**, *4*, 3088–3097. [[CrossRef](#)]
126. ıplak, Z.; Yıldız, A.; Yıldız, N. Green preparation of ternary reduced graphene oxide-au@polyaniline nanocomposite for supercapacitor application. *J. Energy Storage* **2020**, *32*, 101846. [[CrossRef](#)]
127. Fu, X.; Zhang, W.; Lan, B.; Wen, J.; Zhang, S.; Luo, P.; Zhang, R.; Hu, S.; Liu, Q. Polyaniline Nanorod Arrays as a Cathode Material for High-Rate Zinc-Ion Batteries. *ACS Appl. Energy Mater.* **2020**, *3*, 12360–12367. [[CrossRef](#)]
128. Dianat, N.; Rahmanifar, M.S.; Noori, A.; El-Kady, M.F.; Chang, X.; Kaner, R.B.; Mousavi, M.F. Polyaniline-Lignin Interpenetrating Network for Supercapacitive Energy Storage. *Nano Lett.* **2021**, *21*, 9485–9493. [[CrossRef](#)]
129. Kuchena, S.F.; Wang, Y. Superior Polyaniline Cathode Material with Enhanced Capacity for Ammonium Ion Storage. *ACS Appl. Energy Mater.* **2020**, *3*, 11690–11698. [[CrossRef](#)]
130. Adhikari, A.D.; Shauloff, N.; Turkulets, Y.; Shalish, I.; Jelinek, R. Tungsten-Disulfide/Polyaniline High Frequency Supercapacitors. *Adv. Electron. Mater.* **2021**, *7*, 2100025. [[CrossRef](#)]
131. Yavuz, A.; Erdogan, P.Y.; Zengin, H. The use of polyaniline films on flexible tape for supercapacitor applications. *Int. J. Energy Res.* **2020**, *44*, 1–15. [[CrossRef](#)]
132. Korent, A.; Trafela, S.; Soderˆznik, K.Z.; Samardˆzija, Z.; Sturm, S.; Roˆzman, K.Z. Au-decorated electrochemically synthesised polyaniline-based sensory platform for amperometric detection of aqueous ammonia in biological fluids. *Electrochim. Acta* **2022**, *430*, 141034. [[CrossRef](#)]
133. Farooqi, B.A.; Ashraf, A.; Farooq, U.; Ayub, K. Comparative study on sensing abilities of polyaniline and graphene polyaniline composite sensors toward methylamine and ammonia. *Polym Adv. Technol.* **2020**, *31*, 3351–3360. [[CrossRef](#)]

134. Mahalakshmi, S.; Sridevi, V. Conducting, crystalline and electroactive polyaniline-Au nanocomposites through combined acid and oxidative doping pathways for biosensing applications: Detection of dopamine. *Mater. Chem. Phys.* **2019**, *235*, 121728. [[CrossRef](#)]
135. Chen, G.; Zheng, J. Non-enzymatic electrochemical sensor for nitrite based on a graphene oxide–polyaniline–Au nanoparticles nanocomposite. *Microchem. J.* **2021**, *164*, 106034. [[CrossRef](#)]
136. Chaudhary, V.; Chavali, M. Novel methyl-orange assisted core-shell polyaniline-silver nanosheets for highly sensitive ammonia chemiresistors. *J. Appl. Polym. Sci.* **2021**, *138*, 51288. [[CrossRef](#)]
137. Lin, L.; Miao, C.; Weng, S.; Ying, S.; Chen, F.; Ye, C.; Zhuang, H.; You, D. Ternary Pt–Au–FeOOH-decorated polyaniline nanocomposite for sensitive dopamine electrochemical detection. *J. Electroanal. Chem.* **2020**, *877*, 114519. [[CrossRef](#)]
138. Verma, A.; Chaudhary, P.; Singh, A.; Tripathi, R.K.; Yadav, B.C. ZnS Nanosheets in a Polyaniline Matrix as Metallopolymer Nanohybrids for Flexible and Biofriendly Photodetectors. *ACS Appl. Nano Mater.* **2022**, *5*, 4860–4874. [[CrossRef](#)]
139. Hua, M.; Hwang, G.; Chuang, Y.; Chen, S.; Tsai, R. Soluble n-Doped Polyaniline: Synthesis and Characterization. *Macromolecules* **2000**, *33*, 6235–6238. [[CrossRef](#)]
140. Han, Z.; Liu, Q.; Zhao, H.; Shi, Y.; Liu, Y.; Chen, J. Preparation and properties of polyaniline-silver composite by glucose reduction. *Polym. Compos.* **2022**, *43*, 1121–1127. [[CrossRef](#)]
141. Miyashita, R.; Goto, H. Electro-Magneto-Optically Active Polyaniline/Hydroxypropyl Cellulose Composite. *ACS Appl. Polym. Mater.* **2022**, *4*, 796–805. [[CrossRef](#)]
142. Lin, C.; Xue, S.; Ji, C.; Huang, S.; Tung, V.; Kaner, R.B. Conducting Polyaniline for Antifouling Ultrafiltration Membranes: Solutions and Challenges. *Nano Lett.* **2021**, *21*, 3699–3707. [[CrossRef](#)] [[PubMed](#)]
143. Kweon, H.; Lin, C.; Hasan, M.M.F.; Kaner, R.; Sant, G.N. Highly Permeable Polyaniline–Graphene Oxide Nanocomposite Membranes for CO₂ Separations. *ACS Appl. Polym. Mater.* **2019**, *1*, 3233–3241. [[CrossRef](#)]
144. Mondal, S.; Rana, U.; Das, P.; Malik, S. Network of Polyaniline Nanotubes for Wastewater Treatment and Oil/Water Separation. *ACS Appl. Polym. Mater.* **2019**, *1*, 1624–1633. [[CrossRef](#)]
145. Perea-López, N.; Elías, A.L.; Berkdemir, A.; Castro-Beltran, A.s.; Gutiérrez, H.R.; Feng, S.; Lv, R.; Hayashi, T.; López-Urías, F.; Ghosh, S.; et al. Photosensor Device Based on Few-Layered WS₂ Films. *Adv. Funct. Mater.* **2013**, *23*, 5511–5517. [[CrossRef](#)]
146. Lv, S.; Bian, L.; Qiu, J.; Zhang, X.; Gao, M.; He, X.; Ma, X.; Li, G. Surface Modification of Graphene Oxide with Pyrene Derivatives and their Photo-Switching Behaviors. *Mater. Sci. Forum* **2017**, *898*, 1739–1748. [[CrossRef](#)]
147. Gao, M.; Guo, B.; Ma, L.; Zhang, B.; He, X.; Bian, L.; Ma, X.; Li, G. NIR (Near-Infrared) Driven Carbon Nanotube Modified with Dendrimers. *Mater. Sci. Forum* **2016**, *848*, 551–556. [[CrossRef](#)]
148. Ma, X.; Zhang, B.; Cong, Q.; He, X.; Gao, M.; Li, G. Organic-inorganic nanocomposites of ZnO-CuO-chitosan with improved properties. *Mater. Chem. Phys.* **2016**, *178*, 88–97. [[CrossRef](#)]